

EXPERIMENTAL STUDY OF
FINITE-AMPLITUDE STANDING WAVES IN
RECTANGULAR CAVITIES WITH
PERTURBED BOUNDARIES

Ender Kuntsal

NAVAL POSTGRADUATE SCHOOL

Monterey, California



THESIS

EXPERIMENTAL STUDY OF
FINITE-AMPLITUDE STANDING WAVES IN
RECTANGULAR CAVITIES WITH PERTURBED BOUNDARIES

by

Ender Kuntsal

December 1978

Thesis Advisor:

J. Sanders

Approved for public release; distribution unlimited.

T186196

UNCLASSIFIED

SECURITY CLASSIFICATION OF THIS PAGE (When Data Entered)

REPORT DOCUMENTATION PAGE		READ INSTRUCTIONS BEFORE COMPLETING FORM
1. REPORT NUMBER	2. GOVT ACCESSION NO.	3. RECIPIENT'S CATALOG NUMBER
4. TITLE (and Subtitle) Experimental Study of Finite-Amplitude Standing Waves in Rectangular Cavities with Perturbed Boundaries		5. TYPE OF REPORT & PERIOD COVERED Master's Thesis December 1978
7. AUTHOR(s) Ender Kuntsal		6. PERFORMING ORG. REPORT NUMBER
9. PERFORMING ORGANIZATION NAME AND ADDRESS Naval Postgraduate School Monterey, California 93940		8. CONTRACT OR GRANT NUMBER(s)
11. CONTROLLING OFFICE NAME AND ADDRESS Naval Postgraduate School Monterey, California 93940		10. PROGRAM ELEMENT, PROJECT, TASK AREA & WORK UNIT NUMBERS
14. MONITORING AGENCY NAME & ADDRESS (if different from Controlling Office)		12. REPORT DATE December 1978
		13. NUMBER OF PAGES 85
		15. SECURITY CLASS. (of this report) Unclassified
		18a. DECLASSIFICATION/DOWNGRADING SCHEDULE
16. DISTRIBUTION STATEMENT (of this Report) Approved for public release; distribution unlimited.		
17. DISTRIBUTION STATEMENT (of the abstract entered in Block 20, if different from Report)		
18. SUPPLEMENTARY NOTES		
19. KEY WORDS (Continue on reverse side if necessary and identify by block number) Finite-amplitude standing waves		
20. ABSTRACT (Continue on reverse side if necessary and identify by block number) Finite-amplitude standing waves in air at ambient temperature contained within a tuneable, rigid-walled rectangular cavity were experimentally investigated. The effects of various geometrical perturbations on the harmonic content of the observed pressure waveform in the presence of degeneracies were compared to theory. Theory and experiment		

UNCLASSIFIED

SECURITY CLASSIFICATION OF THIS PAGE(When Data Entered)

(20. ABSTRACT Continued)

agreed qualitatively in that shape of the resulting curves have the correct form, but significant differences in the level of the second harmonic were frequently observed.

UNCLASSIFIED

2 SECURITY CLASSIFICATION OF THIS PAGE(When Data Entered)

Approved for public release; distribution unlimited.

Experimental Study of
Finite-Amplitude Standing Waves
in Rectangular Cavities with Perturbed Boundaries

by

Ender Kuntsal
Lieutenant, Turkish Navy
B.S.E.E., Naval Postgraduate School, 1978

Submitted in partial fulfillment of the
requirements for the degree of

MASTER OF SCIENCE IN ENGINEERING ACOUSTICS

from the

NAVAL POSTGRADUATE SCHOOL
December 1978

ABSTRACT

Finite-amplitude standing waves in air at ambient temperature contained within a tuneable, rigid-walled, rectangular cavity were experimentally investigated. The effects of various geometrical perturbations on the harmonic content of the observed pressure waveform in the presence of degeneracies were compared to theory. Theory and experiment agreed qualitatively in that shape of the resulting curves have the correct form, but significant differences in the level of the second harmonic were frequently observed.

TABLE OF CONTENTS

I.	INTRODUCTION -----	7
II.	BACKGROUND AND THEORY -----	9
III.	EXPERIMENTAL CONSIDERATIONS -----	14
	A. APPARATUS -----	14
	B. STRENGTH PARAMETER AND MICROPHONE SENSITIVITY -----	20
	C. FREQUENCY PARAMETER -----	22
	D. HARMONICITY COEFFICIENT -----	22
IV.	DATA COLLECTION PROCEDURES -----	24
	A. PRERUN PROCEDURES -----	24
	B. RUN SEQUENCE AND DATA ANALYSIS -----	24
V.	RESULTS -----	28
VI.	CONCLUSIONS -----	33
	APPENDIX A: CURVES -----	34
	APPENDIX B: TABLES -----	58
	BIBLIOGRAPHY -----	82
	INITIAL DISTRIBUTION LIST -----	84

ACKNOWLEDGMENTS

The generous aid and encouragement of Professors James V. Sanders and Alan B. Coppens is gratefully acknowledged.

Thanks are also due to Mr. Bob Moeller for his assistance in fabricating parts of the cavity.

Sincere thanks also to Lt. Mehmet Aydın for providing the theoretical predictions for comparison with this experiment.

I. INTRODUCTION

In 1968, Coppens and Sanders [1] applied a one-dimensional nonlinear, acoustic wave equation with a dissipative term describing absorbtive losses to rigid-walled, closed tubes with large length-to-diameter ratios. They later expanded this model to incorporate empirically determined losses and phase speeds [2]. The model was further extended to include two-and-three-dimensional cases, which were experimentally investigated in rectangular cavities by Lane [3], Devall [4] and Slocum [5].

One of the significant results of these latter investigations was that the agreement between theory and experiment deteriorated when degenerate modes were present. It was clear that at the stage of development existing at that time, the theory was not able to account for the effect of modes degenerate to members of the family of the driven mode.

The purpose of the research reported in this present thesis was to study the effects of these degeneracies. A rectangular cavity was designed and constructed so that one wall could be moved and secured at various positions to introduce or remove degenerate modes as desired. The primary interest was to make a detailed investigation of finite-amplitude standing waves in air at ambient temperatures in rectangular cavity configurations producing degenerate or

nearly degenerate modes, and compare the results to the present state of the model of Coppens and Sanders.

II. BACKGROUND AND THEORY

The study of the distortion of intense acoustic waves begun in 1968 by Kirchhoff [6] was extended by Lamb [7], Fay [8], [9], and by Keller [10].

The model of Coppens and Sanders [1] deals with finite-amplitude standing waves in rigid walled cavities. It is an extension of the Keck-Beyer approach [11] which makes use of perturbation methods and Fourier series representations of the waveform. Coppens and Sanders extended the perturbation approach to include wall losses predicted by Rayleigh-Kirchhoff [12], and showed excellent agreement with experiments conducted in a rigid-walled tube at low levels of nonlinear interactions. The experimental work by Beech [13] and by Ruff [14] showed that at high excitation levels, a difference developed between theory and experiment. Winn [15] experimentally demonstrated that the Rayleigh-Kirchhoff loss mechanisms were not suitably accurate to describe the phase relationships observed in real tubes. The model was then revised to include empirically determined losses and subsequently investigations by Lane [3], extended the excellent agreement between theory and experiment to higher excitation levels. Devall [4], however, found that if degeneracies existed, the model failed to account for the experimentally observed excitation of non-family modes.

The model of Coppens and Sanders is based on a three-dimensional, nonlinear wave equation with a dissipative term describing absorbtive losses encountered by plane standing waves in rigid walled cavities.

The nonlinear wave equation for a viscous fluid in a rectilinear cavity may be written as [16]

$$c_p^2 \square_L^2 \left(\frac{p}{\rho_0 c_0^2} \right) = - \frac{\partial}{\partial t^2} \left[\frac{\gamma-1}{2} \left(\frac{p}{\rho_0 c_0^2} \right)^2 + \left(\frac{\vec{u}}{c_0} \right)^2 \right] \quad (1)$$

where

c_p = phase speed of sound in air

\square_L^2 = D'lambertian operator with losses

ρ_0 = Equilibrium density of the fluid

$c_0^2 = \left(\frac{\partial p}{\partial \rho} \right)_{\text{at } \rho = \rho_0}$, c_0 = speed of sound in air

$\gamma = \frac{c_p}{c_v}$ = Ratio of specific heats

c_p = specific heat for medium at constant pressure

c_v = specific heat for medium at constant volume

\vec{u} = particle velocity

The non-linear, coupled, transcendental equation applicable to a real, rectangular cavity driven near a resonance is [16]

$$R_n \begin{Bmatrix} \cos \\ \sin \end{Bmatrix} (\phi_n - \theta_n) = NM\beta Q_n \cos \theta_n \left[\frac{1}{2} \sum_{j=1}^{n-1} R_j R_{n-j} \begin{Bmatrix} \cos \\ \sin \end{Bmatrix} \times (\phi_j + \phi_{n-j}) \right. \\ \left. - \sum_{j=1}^{\infty} R_{n+j} R_j \begin{Bmatrix} \cos \\ \sin \end{Bmatrix} \times (\phi_{n+j} - \phi_j) \right] \quad (2)$$

for all $n > 1$, where

R_n = Fourier coefficient of n^{th} harmonic component, normalized such that $R_1 = 1$

ϕ_n = Phase angle of the n^{th} harmonic component where $\phi_1 = 0$

θ_n = $\text{Arctan}(-F_n)$

$F_n = Q \left[(n\omega)^2 - (\omega_n)^2 \right] / (n\omega)^2 \doteq 2Q_n \left(\frac{n\omega - \omega_n}{\omega_n} \right)$

for $\frac{n\omega - \omega_n}{\omega_n} \ll 1$

ω_n = Resonance frequency of a resonance

ω = Driving frequency (near ω_1)

$$Q_n = \frac{\omega_n}{\omega_{nu} - \omega_{nL}} \quad (3)$$

$\omega_{nu} - \omega_{nL}$ = Difference of the half power frequencies above and below the fundamental

N = $1/2$ for a one-dimensional standing wave,
 $1/4$ for a two-dimensional standing wave,
 $1/8$ for a three-dimensional standing wave

$$M = \text{Mach number} = \frac{P_1}{\rho_0 c_0^2}$$

P_1 = Peak pressure of fundamental component of wave

$$\beta = (\gamma + 1)/2 \quad \text{for a gas.}$$

The values of Q_n and ω_n are to be experimentally determined from the infinitesimal-amplitude behavior of the cavity.

For perturbed boundaries, the total pressure near resonance is [16]

$$p = (n, m, l / \omega, \theta) - \frac{\epsilon}{\left(\frac{\omega}{c_0}\right)^2 L_x} \sum_{\substack{n=0 \\ m=0 \\ l=0}}^{\infty} a_{ml} \Delta n (-1)^n S_{nml}(n, m, l / \omega, \theta + \sigma_{nml}) \quad (4)$$

where the second term is the first-order perturbation correction and

$(n, m, l / \omega_1 \theta)$ = A standing wave designation when the (n, m, l) mode is driven at angular frequency ω ; θ is the phase angle with respect to $t = 0$

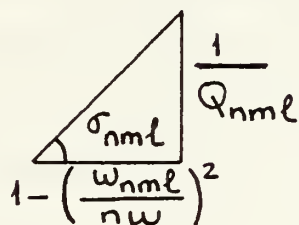
L_x = The width of the cavity

a_{ml} = Fourier coefficients

$$S_{nml} = \frac{Q_{nml}}{\sqrt{1 + F_{nml}^2}} = Q_{nml} \sin \sigma_{nml}$$

$$F_{nml} = \cot \sigma_{nml}$$

and σ_{nml} angle is defined as:



$$\epsilon = \frac{\Delta}{L_x}$$

Δ = Amplitude of the perturbation

$\Delta n = 1$ for $n = 0$, 2 for $n = 1, 2, 3, \dots$

A computer program [16] was made for the solutions of equations (2) and (4). The inputs of this computer program are, Q 's, E 's of the modes (where the E 's will be defined in Section III.D), cavity dimensions, and amplitude of perturbation for each configuration.

III. EXPERIMENTAL CONSIDERATIONS

A. APPARATUS

The rectangular cavity used in this research (Figure 1) was constructed from 0.982 in. milled aluminum plates. The interior of the cavity was 12.002-in. long and 2.502-in. high, while the width could be varied from approximately 5.50 in. to 7.00 in. in 0.25-in. increments. All joints were right angles, to which a thin layer of silicon grease was applied prior to assembly to hermetically seal the cavity. Table I shows the theoretically predicted normal mode frequencies for ideal rectangular cavities corresponding to the seven nominal configurations. Figure 2 explains the modal designations by indicating the nodal planes for a few of the lower modes. Note that, of the 12" x 60" x 2.5" configuration the (100) and (020) modes are theoretically degenerate. Actual measurements of this configuration showed the resonance of the (100) mode to be 6 Hz below that of the (020) mode. To adjust the degree of degeneracy in finer increments, 0.04 in. shims could be attached with rubber cement to the long side of the cavity. With one shim in place the (100) mode was 3 Hz above that of the (020) mode.

Three types of geometrical perturbations were used.

(a) The long wall was machined at a small angle (as shown in Fig. 3) so that in plane view the cavity had a slight

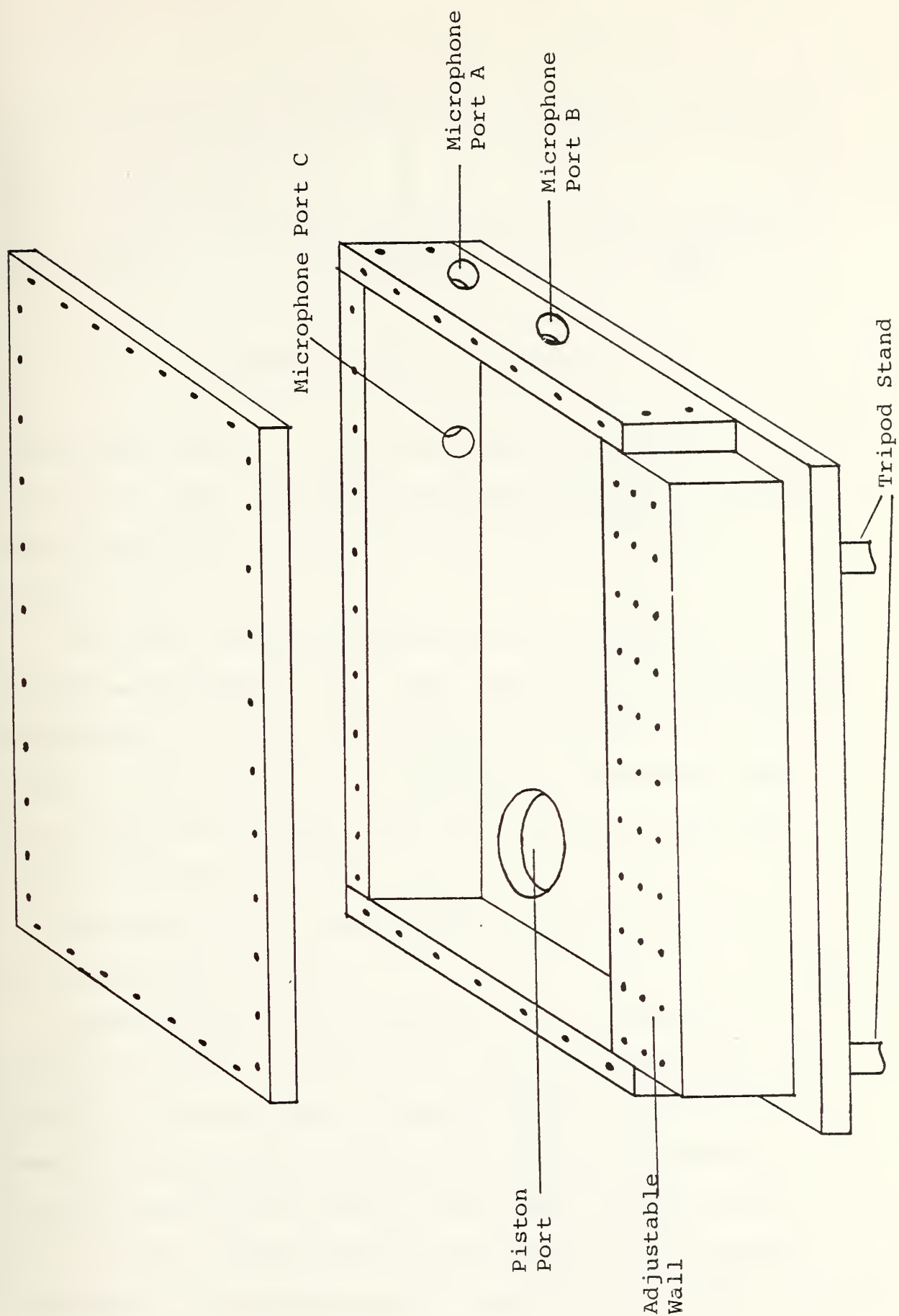


FIGURE 1. ADJUSTABLE RECTANGULAR CAVITY

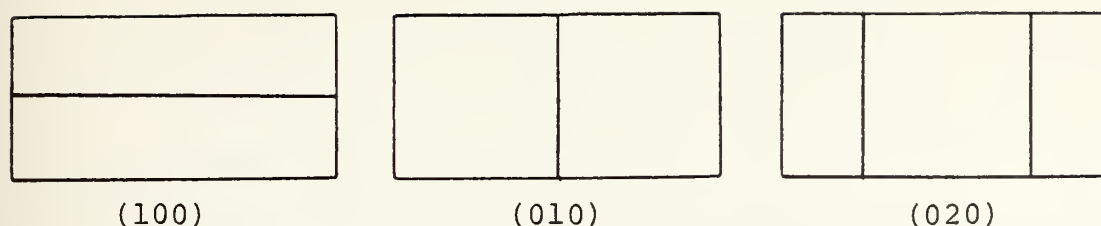


FIGURE 2. MODAL DESIGNATIONS

trapezoidal shape. (b) The long wall was machined as shown in Fig. 4. And, (c) Shims of various widths were cemented to the long side of the cavity at various positions, (Fig 6, f-i).

The effect of these geometrical perturbations on the resonance frequency of the (100) mode could be estimated by calculating an "effective" width of the perturbed cavity from $\Delta L = V/A$, where ΔL is the change in effective width due to the perturbation, and V and A are the volume and area of the perturbation.

The effect of the geometrical perturbation on (4) was calculated in [16].

Acoustic waves were introduced into the cavity by means of a piston located in a 2.25-in. diameter port in the floor of the cavity. A single lubricated O-ring was used to produce a seal between the piston and the port. On the side walls of the cavity three other ports were used for a 1/4-in. diameter Bruel and Kjaer type 4136 condenser microphone. The microphone was mounted in an 0.5-in. diameter

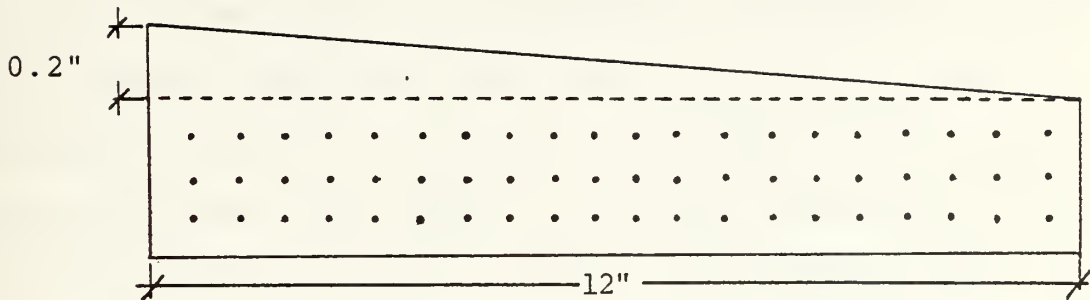


FIGURE 3. LINEARLY PERTURBED WALL

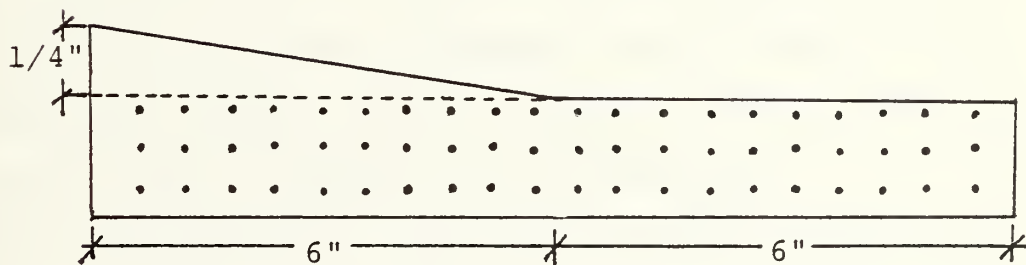
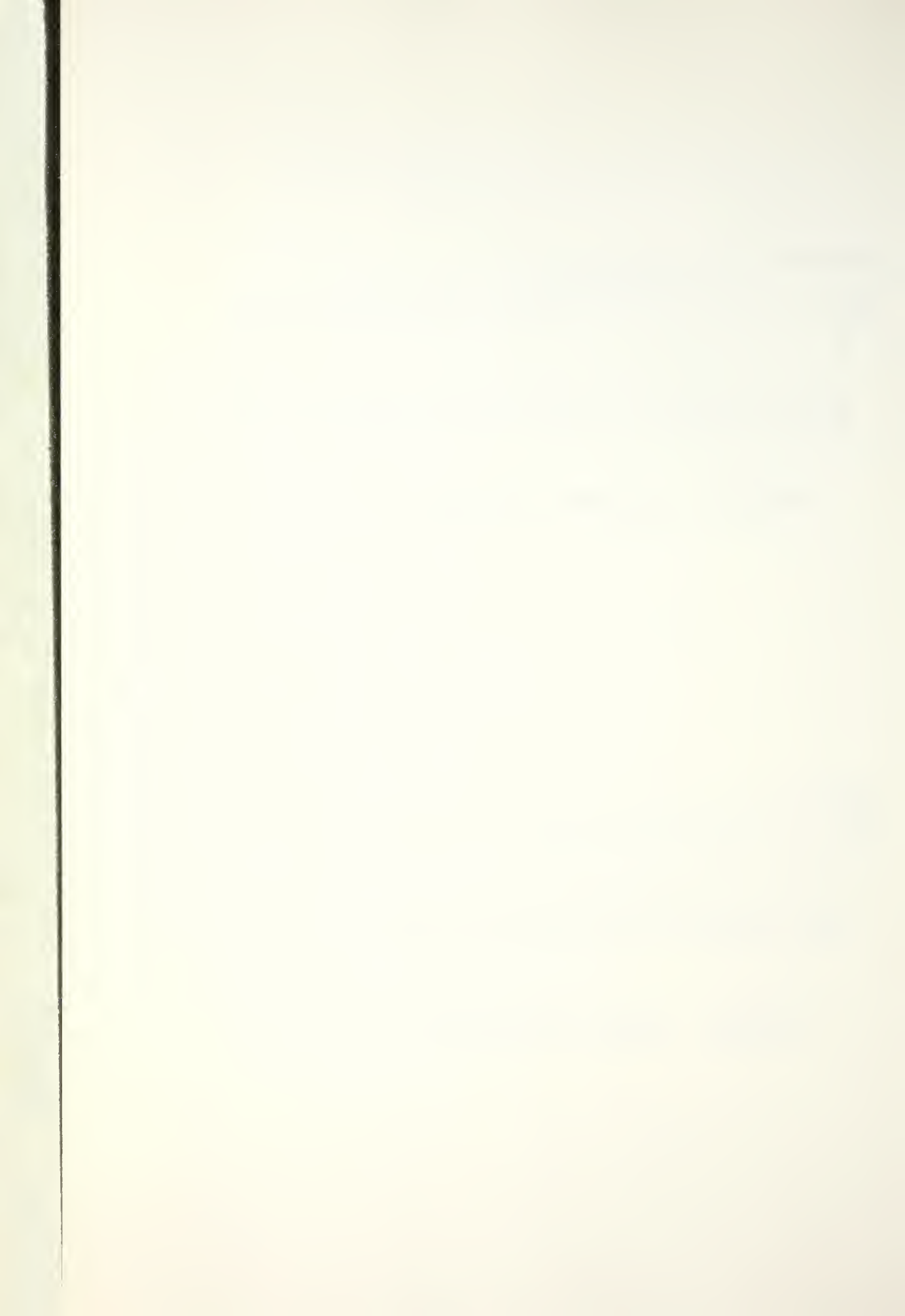


FIGURE 4. WEDGED PERTURBATION



aluminum case and two O-rings and silicone grease were used between this case and the ports for sealing.

The cavity was specifically designed to study the effects of a degeneracy or near degeneracy between the (020) and (100) modes, where the (020) mode is a standing wave with nodes at 2 and 8 in. along the long wall (12 in.) of the cavity and the (100) mode is a standing wave with one node in the middle of the 6 in. wall. To determine the resonance properties of these degenerate modes a microphone port was placed at a node of each of the modes. With the microphone at the node of the (020) mode, the properties of the (100) mode could be measured, and vice versa. A third microphone position, as close to the corner opposite the piston as possible, was used to make the finite amplitude measurements. The axes of the piston and microphone were mutually perpendicular to minimize coupling the mechanical vibration. Since only one microphone was available, two plugs were used to seal the unused ports. Both of these plugs had two small O-rings to provide sealing.

A block diagram of the apparatus is shown in Figure 5.

The piston was driven by an M-B Electronics Model EA1500 exciter which in turn was driven by an M-B Electronics model 2120MB Power Amplifier. The driving signal was produced by a General Radio 1161-A Coherent Decade Frequency Synthesizer, configured to provide frequencies precise to 0.001 Hz.



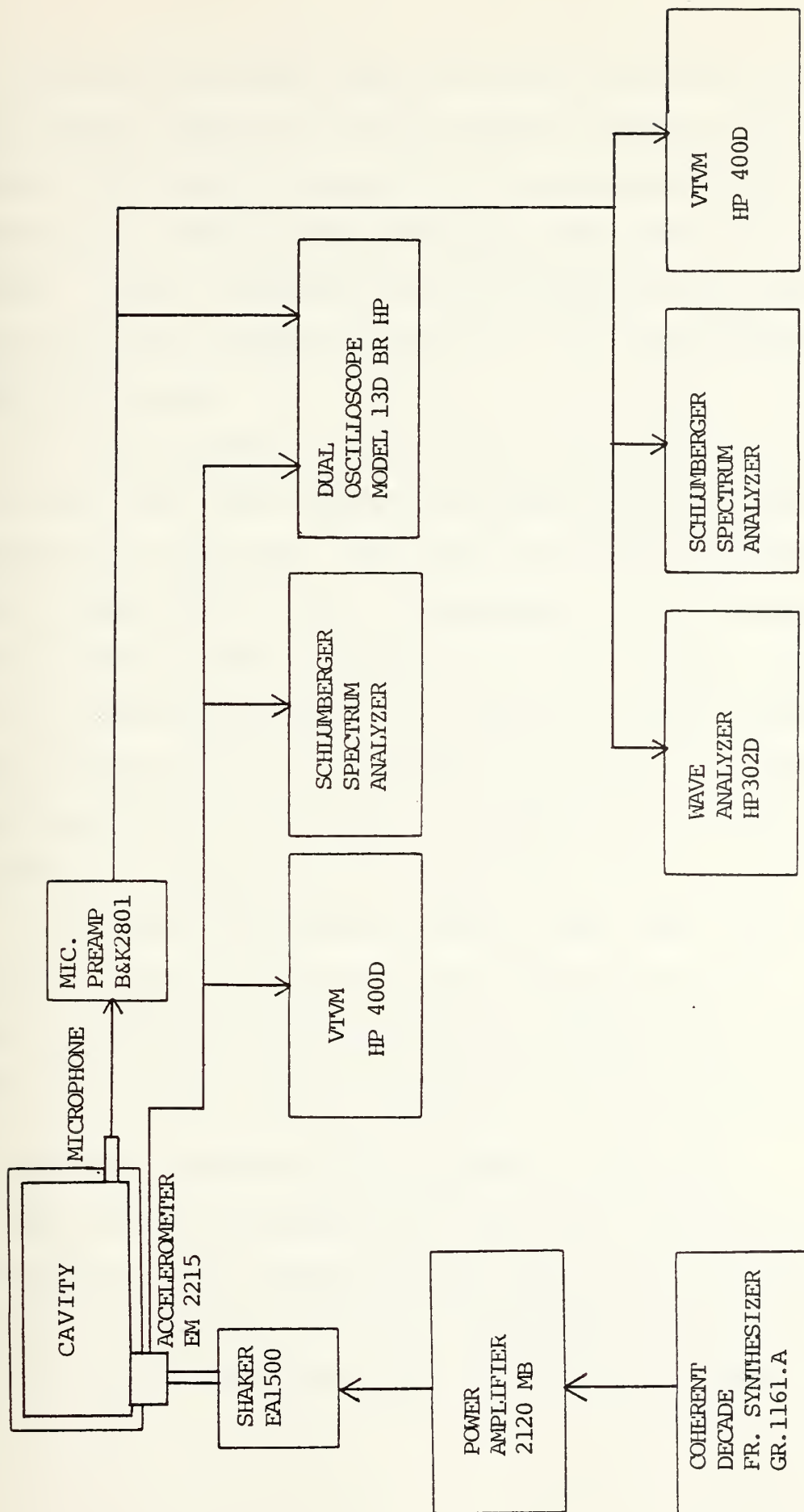
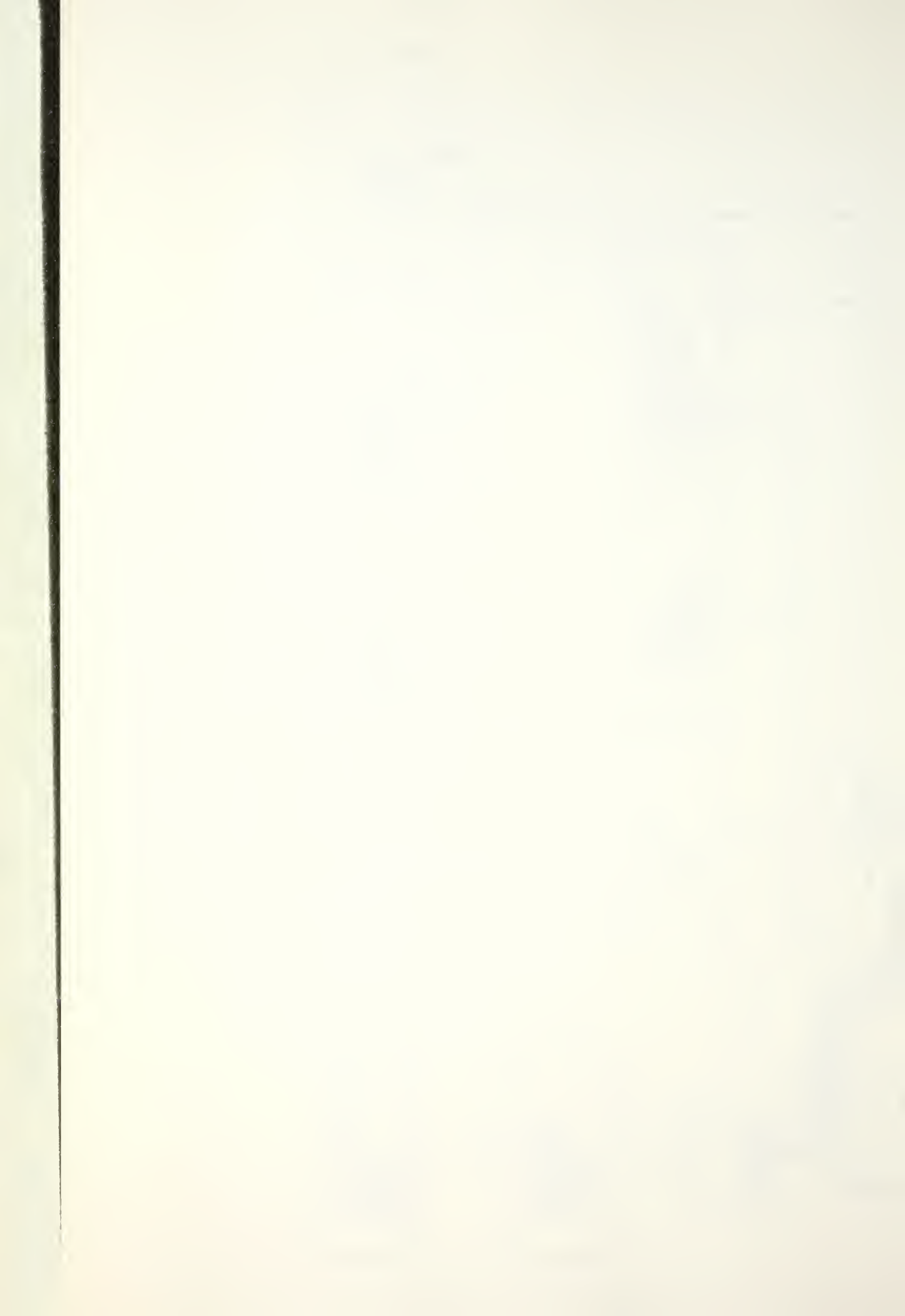


FIGURE 5. APPARATUS BLOCK DIAGRAM



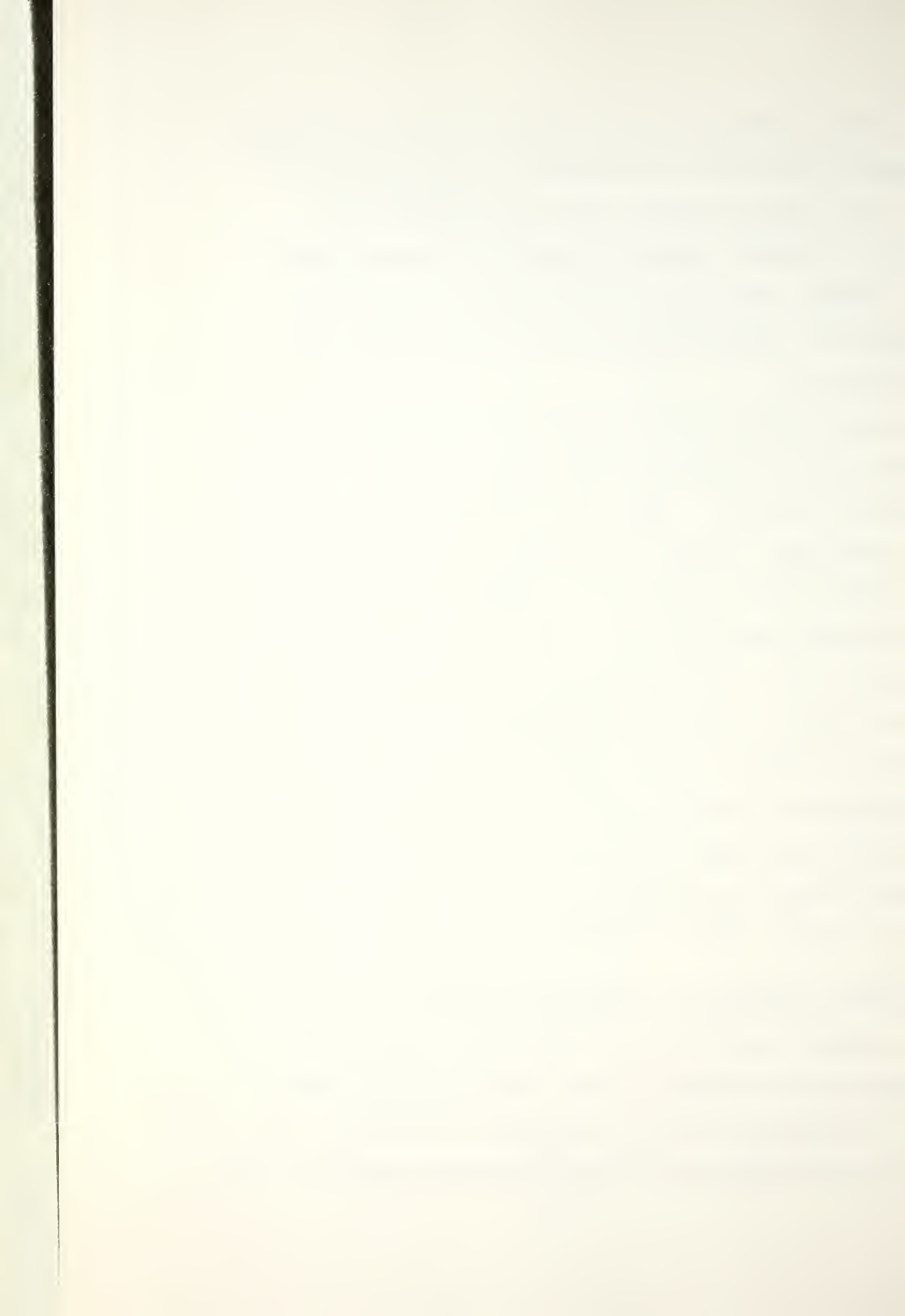
The piston movement was continuously monitored by means of an Endevco Model 2215 Accelerometer mounted within the piston. The output voltage of this accelerometer was measured on a Hewlett Packard Vacuum Tube Voltmeter Model HP400D. Before every data run the output of this meter was checked for harmonic distortion by the Schlumberger Spectrum Analyzer.

The sound pressure in the cavity was sensed by a Bruel. and Kjaer type 413b condenser microphone with matching preamplifier type 2801. The output of this preamplifier went to three other pieces of equipment: (1) a Hewlett Packard HP400D VTUM to measure the overall voltage level, (2) the Spectrum Analyzer, (3) a Hewlett-Packard HP302A Wave Analyzer with 7 Hz bandwidth set to AFC (Automatic Frequency Control), so that it automatically followed the fundamental frequency as the frequency slowly varied.

To minimize the possible effects that could occur due to the vibration coupling of the cavity and exciter, the cavity and exciter were mechanically isolated by placing them on a 5/16-in. sheet of rubber acoustic isolation pad.

B. STRENGTH PARAMETER AND MICROPHONE SENSITIVITY

The strength parameter SP is the basic quantity which characterizes the strength of the finite-amplitude interaction. To determine SP, it is necessary to know P_1 , which in turn can be calculated from the microphone output voltage



V_1 if the microphone sensitivity S_M is known. The microphone sensitivity, obtained with a Bruel and Kjaer model 4220 pistonphone, was

$$S_M = (1.56 \pm 0.03) \times 10^{-3} \text{ Volt}/(\text{N}/\text{m}^2)$$

Then, using

$$SP = M\beta Q_1$$

where $M = \frac{P_1}{\rho c^2}$

$$P_1 = \frac{V_1 \sqrt{2}}{S_M}$$

$$\rho = 1.293 \text{ kg./m}^3$$

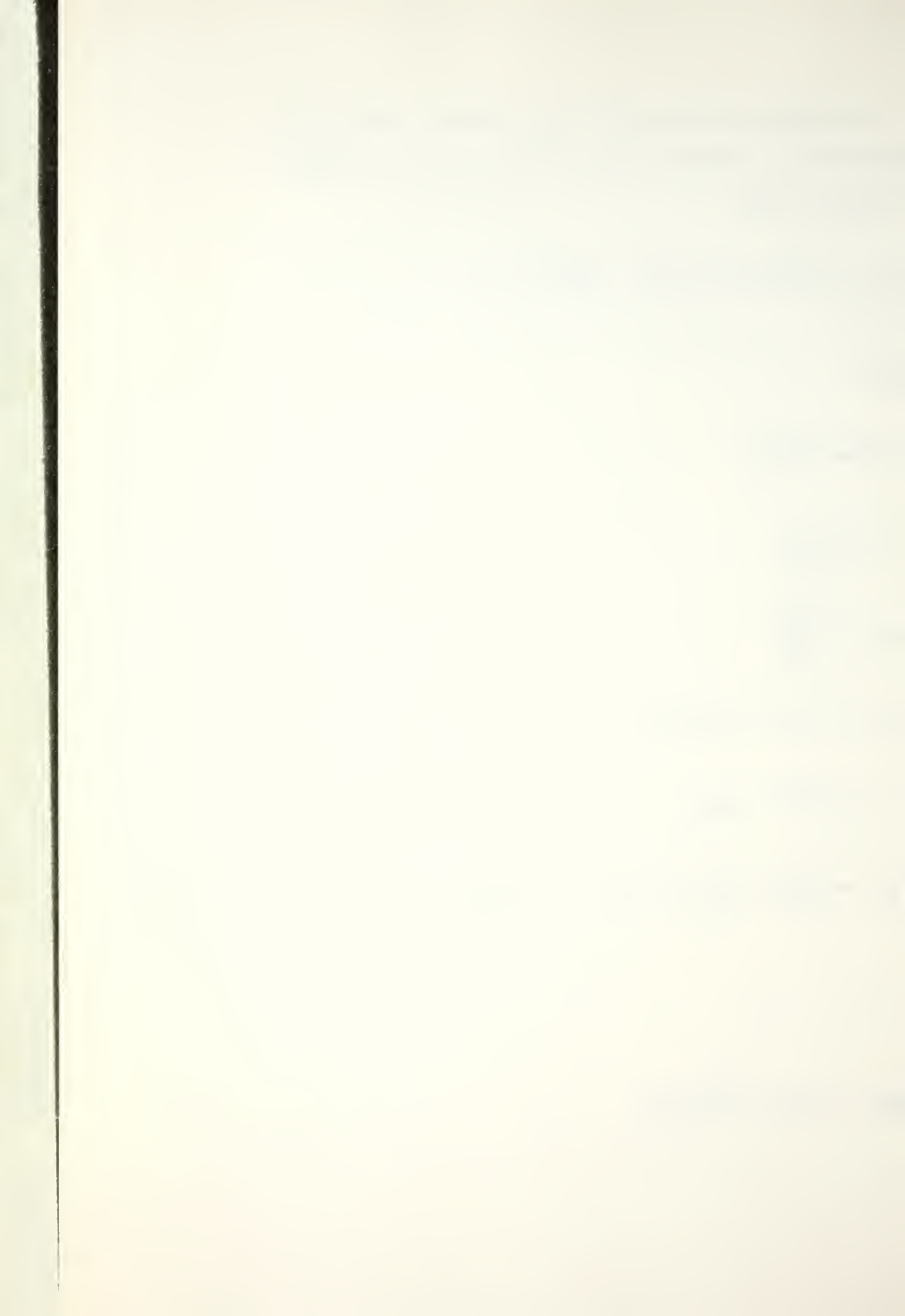
$$c = 345 \text{ m/sec}$$

$$\beta = \frac{1}{2} \left(1 + \frac{C_P}{C_V} \right) = 1.2 \quad \left(\frac{C_P}{C_V} = 1.4 \right)$$

we have,

$$SP = 7.07 \times 10^{-3} V_1 Q_1$$

(5)



where

V_1 = RMS voltage output of the first harmonic
at the microphone, and

Q_1 = Q value of the driven mode.

C. FREQUENCY PARAMETER

The frequency parameter, defined by

$$FP = 2Q_1(f - f_1)/f_1 \quad (6)$$

normalizes the driving frequency f to the corresponding resonance frequency f_1 of the system. For example, FP equal to ± 1.00 corresponds to driving the cavity at the 1/2-power points of the fundamental resonance.

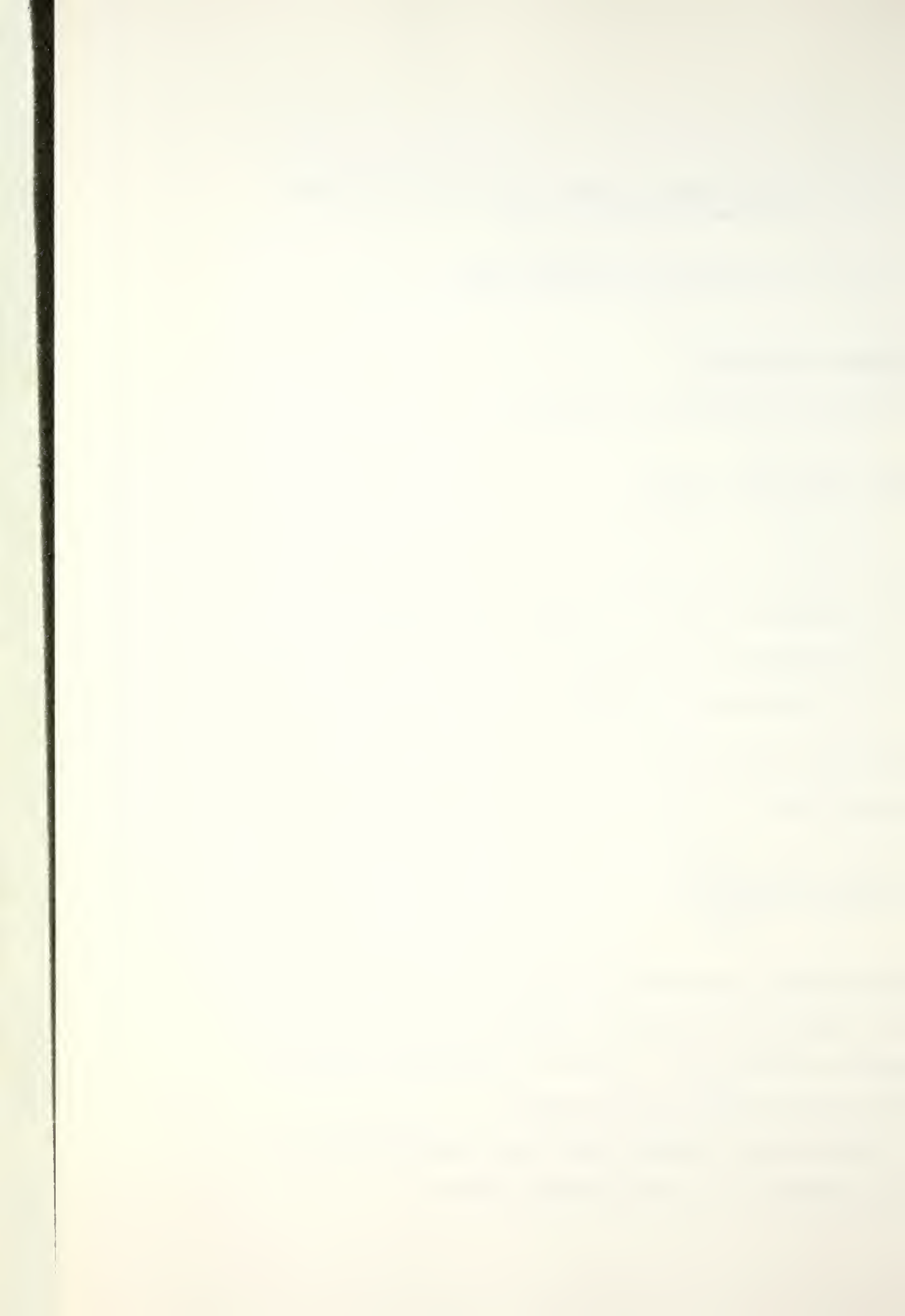
D. HARMONICITY COEFFICIENT

A quantity $E(n)$, defined by

$$E(n) = \frac{f_n - nf_1}{nf_1} \quad (7)$$

indicates how well the modes of a given family are tuned, i.e., how closely the resonance frequency of the n th mode of the family agrees with n times the resonance frequency f_1 of the gravest member of the family.

The relationship between harmonicity coefficient and frequency parameter is approximately given as



$$FP \doteq 2Q_n E(n)$$

IV. DATA COLLECTION PROCEDURES

A. PRERUN PROCEDURES

To keep frequency drift to a minimum, the system was warmed up at least one hour prior to data collection. After this warmup period the piston was adjusted so that the harmonic content of the accelerometer output as analyzed on the Schlumberger Spectrum Analyzer was at least 50 dB down from the fundamental.

To keep the strength parameter, i.e., V_1 , constant as the driving frequency was changed it was necessary to drive the piston at greater amplitudes for frequencies away from the resonance frequency. Since this tended to produce greater harmonics content in the piston motion, it was necessary to use rather low strength parameters when the experimental plan required measurements at frequencies far (>5 Hz) from resonance.

B. RUN SEQUENCE AND DATA ANALYSIS

Data were collected in three parts: a pre-run infinitesimal-amplitude measurement, the finite amplitude run, and a post-run infinitesimal amplitude measurement. The tables in Appendix B show the data collected. During the pre-run infinitesimal amplitude measurement, the piston was driven at less than 0.1V (rms). Because the (100) and (020) modes were nearly degenerate, measurement of the properties of the (100) mode were made with the microphone in port C,

while measurements of the (020) mode were made with the microphone in port B. All nondegenerate modes were measured at port A. The resonance frequency f_r of a mode was found from

$$f_r = \frac{f_u + f_L}{2}$$

the Q from

$$Q = \frac{f_r}{f_u - f_L}$$

and the harmonicity coefficient from

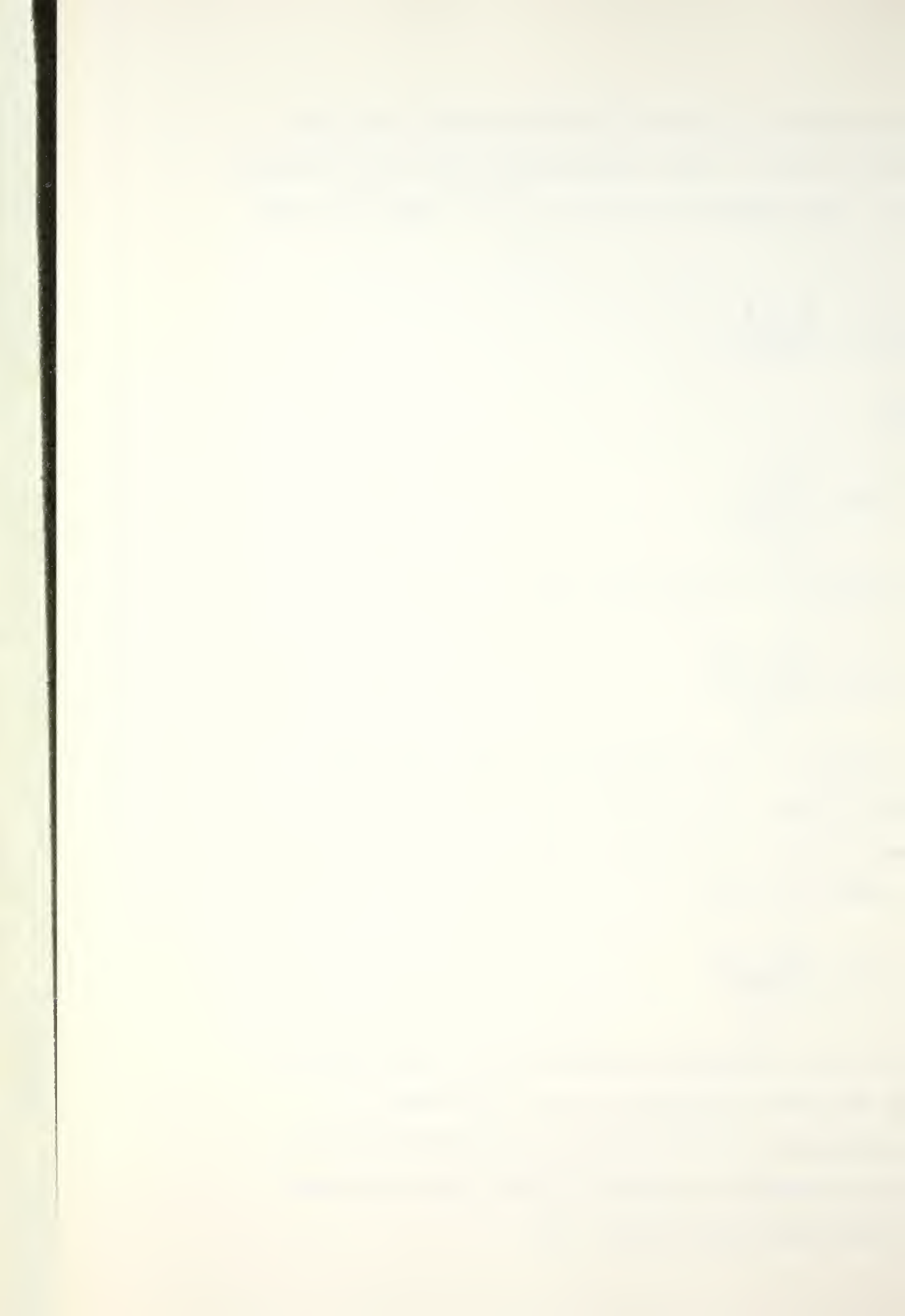
$$E = \frac{f_n - n f_1}{n f_1}$$

where f_u and f_L are the frequencies of the upper and lower half-power points, and f_n is the resonance frequency of the n th member of the (010) family. An E is also calculated for the (100) mode from

$$E = \frac{f_r - f_2}{f_2}$$

where f_r is the resonance frequency of the (100) mode and f_2 is the resonance frequency of the (020) mode.

The microphone output voltage V_1 necessary to obtain the strength parameter required for the finite-amplitude run was then calculated from Eq. (5).



All finite-amplitude measurements were made at port A. To keep the strength parameter the same for all frequencies, it was necessary to adjust the driving voltage applied to the piston so that the microphone output voltage V_1 , as measured on the HP302A Wave Analyzer, remained constant. During the run the frequency was increased in 0.3 Hz. steps at 5 or 3 minute intervals. At each driving frequency, the harmonic content of the microphone output was measured with the Schlumberger Spectrum Analyzer.

During the post-run infinitesimal-amplitude measurement, the pre-run procedure was repeated. The values of Q and E used for input to the theory were the average of the pre- and post-run measurements.

The finite-amplitude results are presented as the percent harmonic as a function of frequency parameter for a given strength parameter and given perturbation. The percent harmonic in the microphone output was found by taking the voltage levels VL_n read on the Schlumberger Spectrum Analyzer and converting them to voltages V_n by

$$V_n = 100 \times 10^{-\frac{VL_n}{20}} \quad (mV)$$

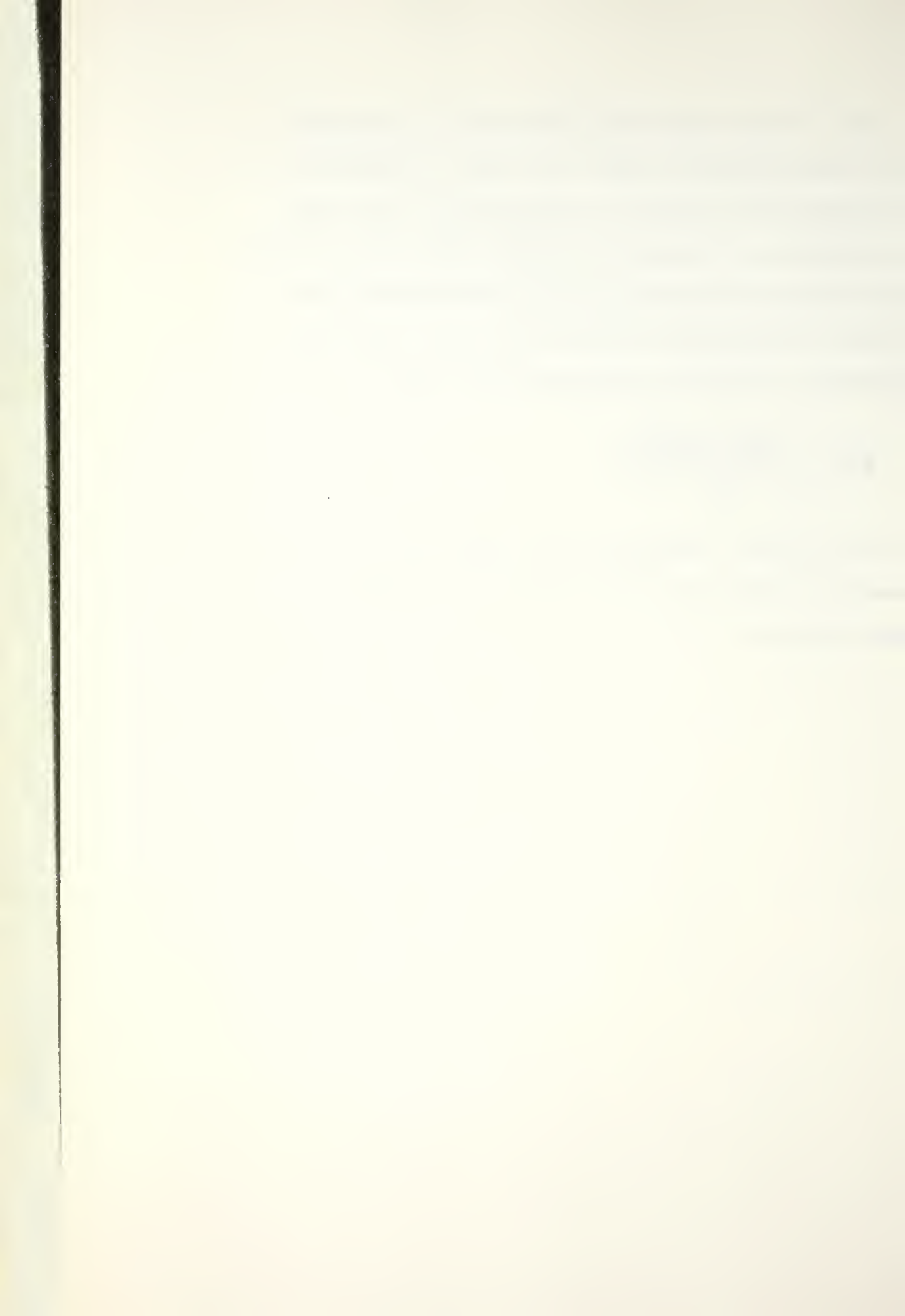
and then dividing by V_1 . To find the frequency parameter to sufficient accuracy it was necessary to know the resonance frequency of the (010) mode at the instant the finite-amplitude measurement was made. Previous investigations



[3], [4], and [5] have shown that the drift in resonance frequency is approximately linear with time. Therefore, the pre- and post-run resonance frequencies for the (010) mode were plotted vs. time and a straight line drawn between them. The resonance frequency at any time between these two runs could be estimated directly from this graph and the corresponding frequency parameter found from

$$FP = \frac{2Q_1(f-f_1)}{f_1}$$

where f is the driving frequency and f_1 the value of the (010) resonance frequency at the time the finite-amplitude measurement was made.



V. RESULTS

Figure 6 shows the cavity configurations investigated in this thesis. All shims are 0.04-in. thick and reach from the floor of the cavity to its ceiling.

Figure 7 shows the infinitesimal amplitude response of the unperturbed cavity for configuration a. At port A, both the (100) and (020) modes are observable with their resonance peaks separated by 6 Hz. At port B the (020) mode predominates but the (100) mode is still apparent. At port C the (100) modes predominates with only a small amount of the (020) mode present. Figure 7 shows the results of the finite-amplitude theory and experiment of this unperturbed configuration. The strength parameter (STRPM) is 0.399. This and the cavity parameters used in the theory are shown at the top of this figure. The continuous lines are the theoretical predictions and the \square are the experimental results. The theory and experiment are in good agreement and the observed differences are within experimental error as determined from repeated runs.

Figure 9 shows the results for the perturbed cavity (configuration b). The theory predicts no excitation of non-family modes by a perturbation of this form and none is observed experimentally. Again the theory and experiment agree to within the expected experimental error. (The behavior of the third harmonic for frequency parameters less

than -2 is probably due to third harmonic introduced into the cavity by the piston which must be driven very hard this far from resonance.)

Figures 10 and 11 show the results for configuration c. The thin continuous line shows the theoretical predictions without applying the perturbation correction and the thick continuous line shows the predictions with the perturbation correction. For the second harmonic, the frequency at which the effect of the perturbation occurs and the magnitude of this effect predicted by the theory are in good agreement with the experiment. However, there is a large discrepancy between the magnitude of the predicted and experimental second harmonic which disappears on the side of the curve away from the perturbation. The third harmonic is so weak that it is impossible to make any comments about it.

If the cavity wall is moved back, thereby separating the degenerate modes by 45 Hz, as shown in Fig. 12, the effect of the perturbation, as predicted by theory, is very small (Fig. 13), but the experiment shows a significant difference in magnitude from the predictions - again on the side of the curve adjacent to the perturbation.

The infinitesimal-amplitude curves for configuration d are shown in Fig. 14. The volume of this shim is such that the (100) and (020) modes are almost exactly degenerate. Figure 15 compared to Fig. 14 shows that the location of the shim has no noticeable effect on the resonance frequencies.

To separate the degenerate modes, a "full" shim was placed on the long wall of the cavity (configuration e). The infinitesimal-amplitude curves for this configuration are shown in Fig. 16. The two modes are 3 Hz apart. If a perturbation is now introduced by another shim (configuration f), the resonance frequencies are 9 Hz apart (Fig. 17), and the finite-amplitude results are shown in Fig. 18. The agreement between theory and experiment is only qualitative. The effect of the perturbation appears at the right frequency parameter but the magnitude appears to be wrong. At frequency parameters greater than 4.7, where the effect of the perturbation maximizes, the experimental results decrease more rapidly than predicted. The different frequency parameters at which the theory and experiment achieve their principle maximum may be the result of experimental uncertainties or it may be a further indication of the qualitative failure of the prediction.

Moving the shim to the side wall (configuration g) does not alter the infinitesimal-amplitude behavior, but it does make the theoretical perturbation correction go to zero. Figure 19 shows the finite-amplitude results for this configuration. The behavior of the experimental results probably indicate that extraneous harmonic is being introduced by the large driving amplitudes needed far from resonance.

To bring the resonance frequencies of the two modes closer together a smaller shim was used (configuration h).



The infinitesimal-amplitude behavior is shown in Fig. 20. The modes are now 6 Hz apart instead of 9 Hz. The finite amplitude results are shown in Fig. 21. Once again the agreement is qualitative but there seems to be a significant quantitative disagreement. This disagreement may be caused by the fact that the perturbation correction B , for configuration h is 0.274 which is much larger than that for which the theory should be accurate ($B < 0.1$). To test this hypothesis the perturbation correction was reduced ($B = 0.134$) by moving the shim towards a corner (Fig. 22). Now the effect of the perturbation as predicted by the theory is almost indistinguishable from the prediction with no perturbation (i.e., the thick and thin lines are almost identical), but there is a noticable experimental effect for the second harmonic. The agreement between theory and experiment for frequency parameters away from that near the perturbation is now excellent.

To bring the resonances even closer together, the size of the shim was further reduced and its position was adjusted to produce $B = 0.0467$ (configuration i). Figure 23 shows the resonance 5 Hz apart down from 6 Hz in the previous configuration. Figure 24 shows that the effect of this perturbation is predicted to be greater than for the previous configuration and that the agreement between theory and experiment is not as good as for configuration h .

The effects of increasing B further ($B = 0.148$) are shown in Fig. 25. The agreement between theory and experiment

deteriorates further, but the general characteristics of the disagreements between theory and experiment are the same as observed in all previous configurations.

To investigate how these differences between theory and experiment depend on the position of the (100) resonance with respect to the (020) resonance, configuration j was used to move the (100) resonance to the low frequency side of that of the (020) resonance (Fig. 26). Figure 27 shows that the effects are very much the same for the second harmonic. Once again the third harmonic seems to be in complete disagreement with the predictions of the theory. Figure 28 shows the effect of increasing the strength parameter to 0.29 (from 0.205 in Fig. 27). The agreement between experiment and theory is much better.

VI. CONCLUSIONS

The experimental apparatus used in this thesis is ideally suited for the study of the effects of geometrical perturbations on the finite-amplitude behavior of standing waves. While the use of a shim to provide the perturbation is convenient and flexible, other forms of perturbation should be studied to determine if the form of the perturbation has any influence on the degree of agreement between theory and experiment.

For the perturbations studied, theory and experiment agreed qualitatively in that the effect occurred at the correct frequency parameter and the shape of the curve was of the same as predicted. However, a significant difference in the level of the second harmonic was observed over most of the range of frequency parameters for most cases studied with the experimental levels being less than predicted by the theory. The exception to this statement is one run made at a higher strength parameter where the agreement between theory and experiment was excellent over most of the curve. In all cases, the observed correction in the region of the degenerate mode was larger than predicted.

The behavior of the third harmonic was erratic and seldom bore any relation to predictions. The levels of the measured third harmonic were very low and this may have been a "signal-to-noise" problem, but the behavior of the third harmonic deserves further study.



APPENDIX A
CURVES

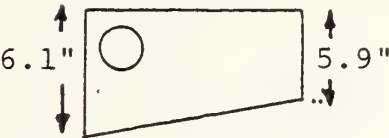
Cavity Configuration

Cavity

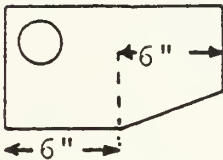
a



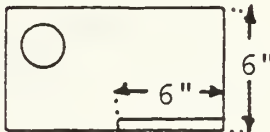
b



c



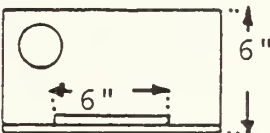
d



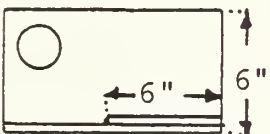
e



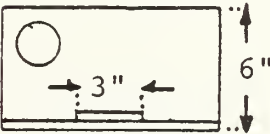
f



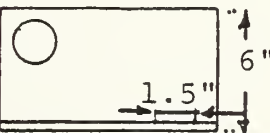
g



h



i



j



FIGURE 6



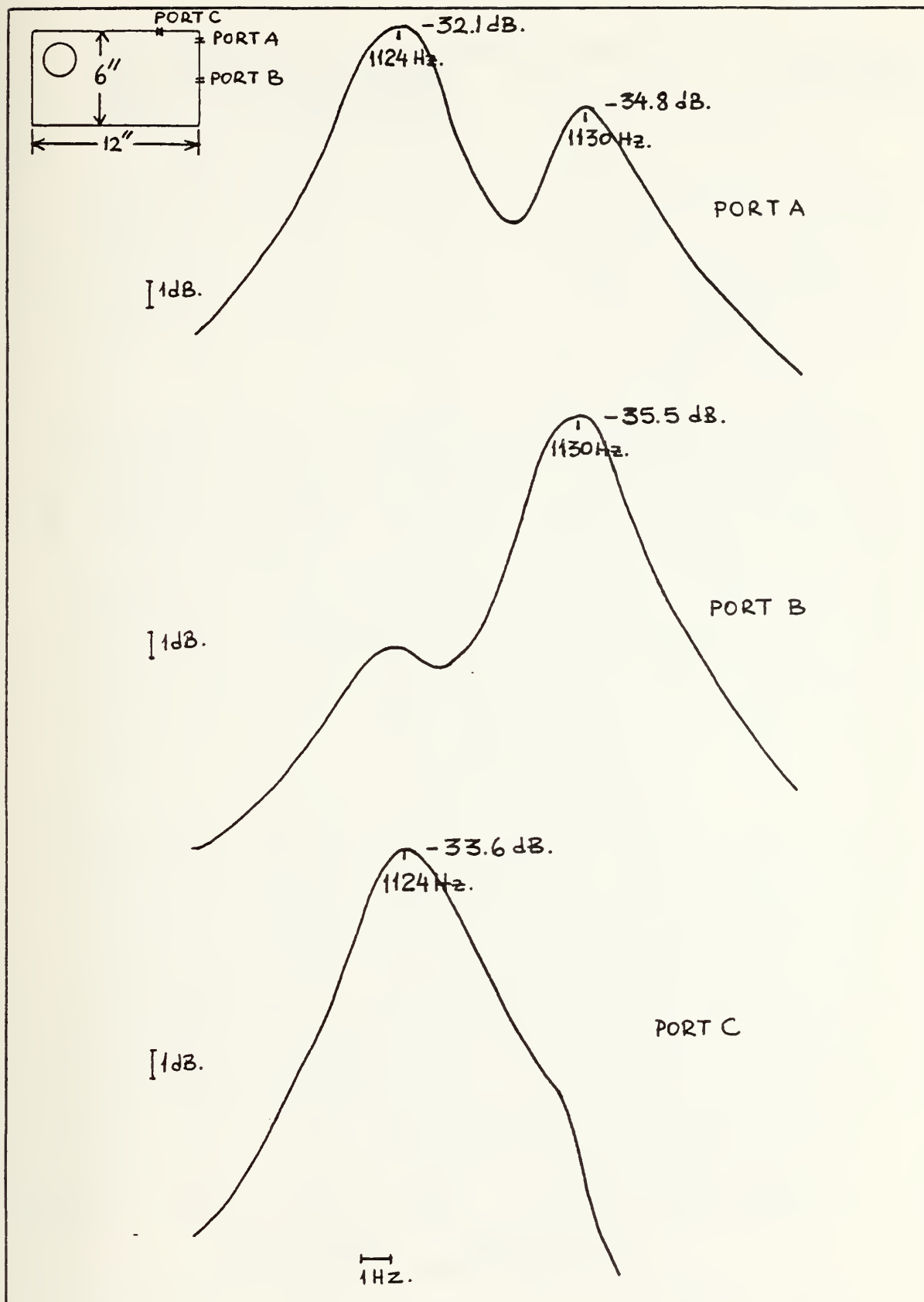
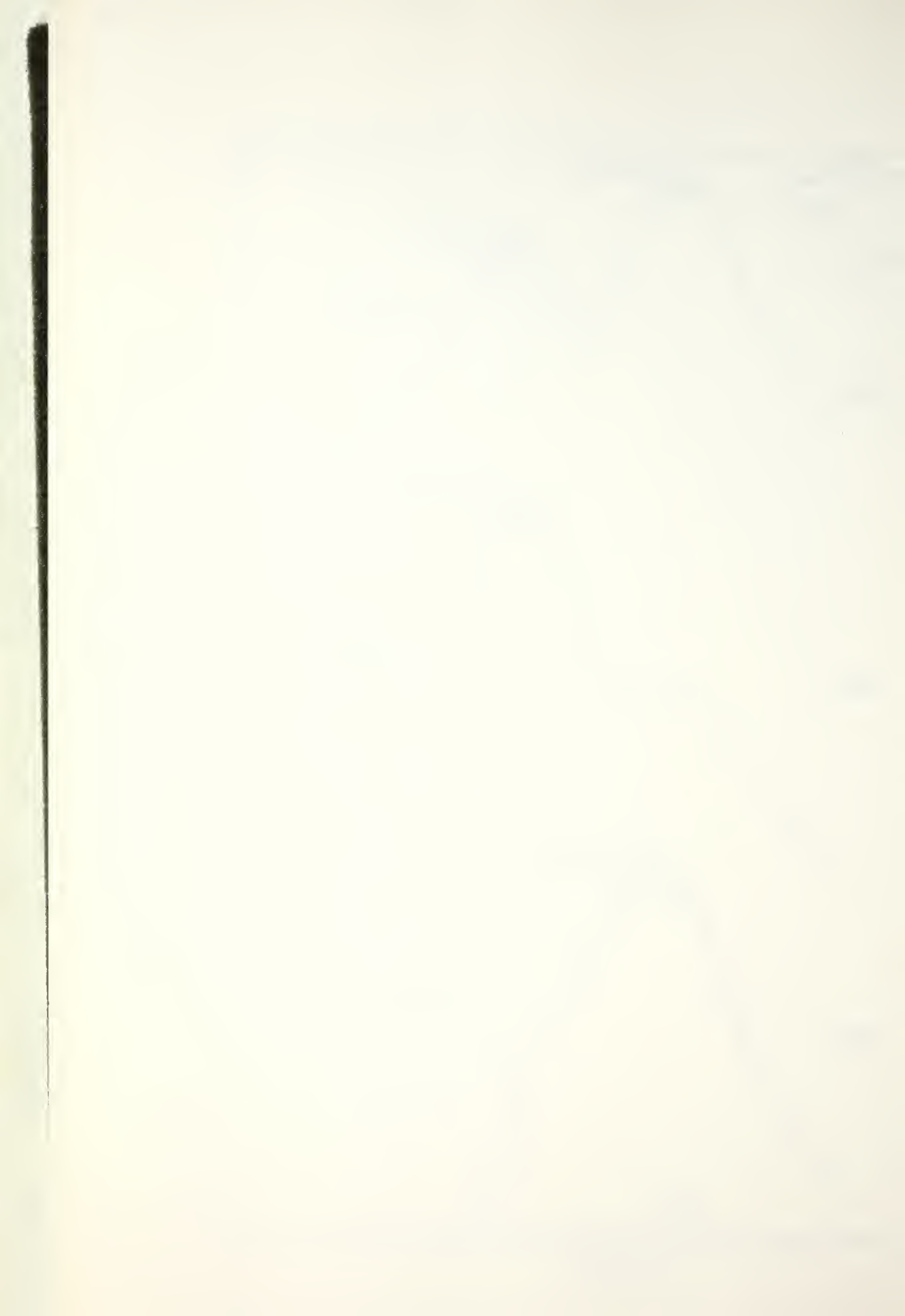


FIGURE 7



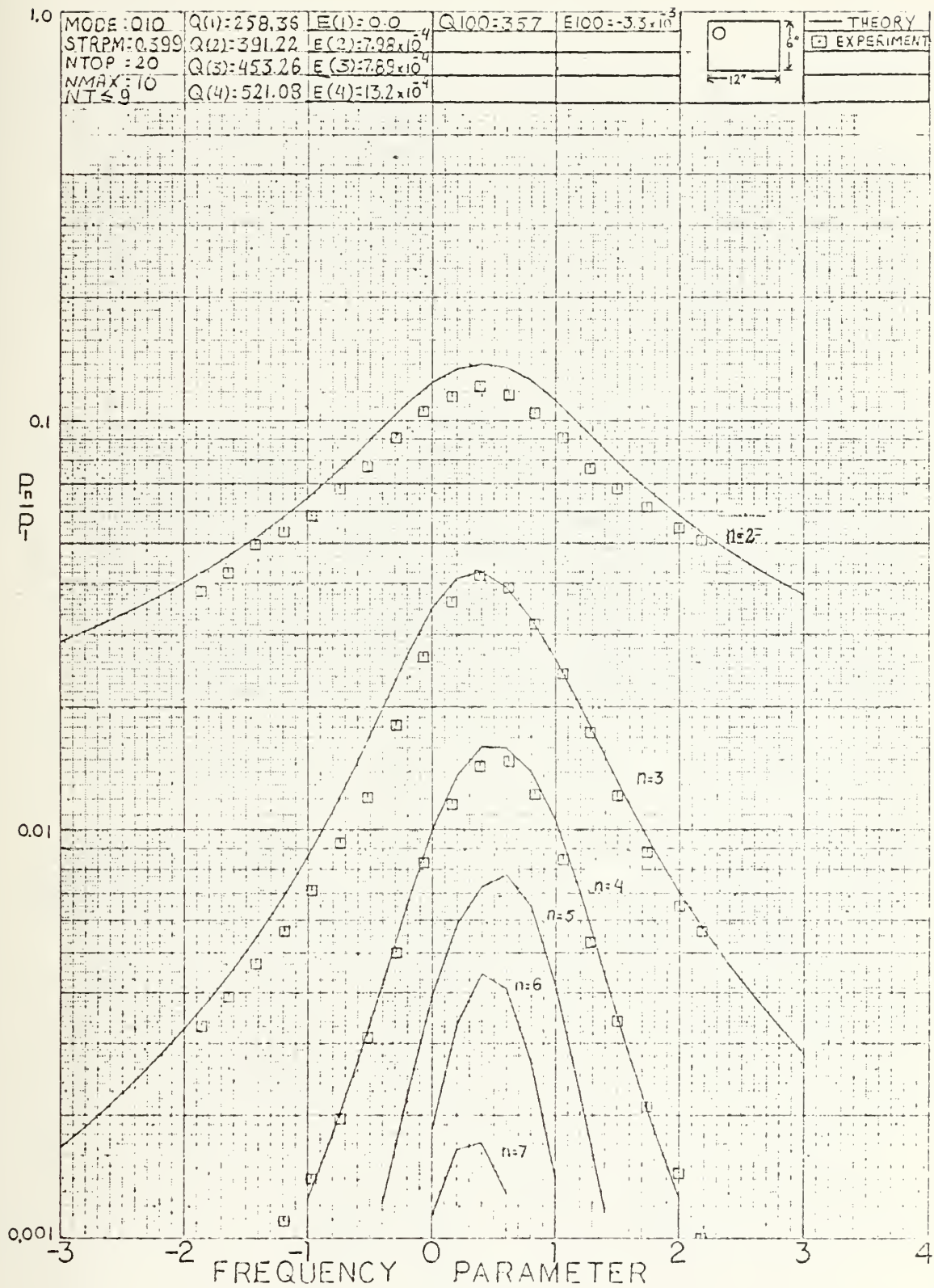


FIGURE 8

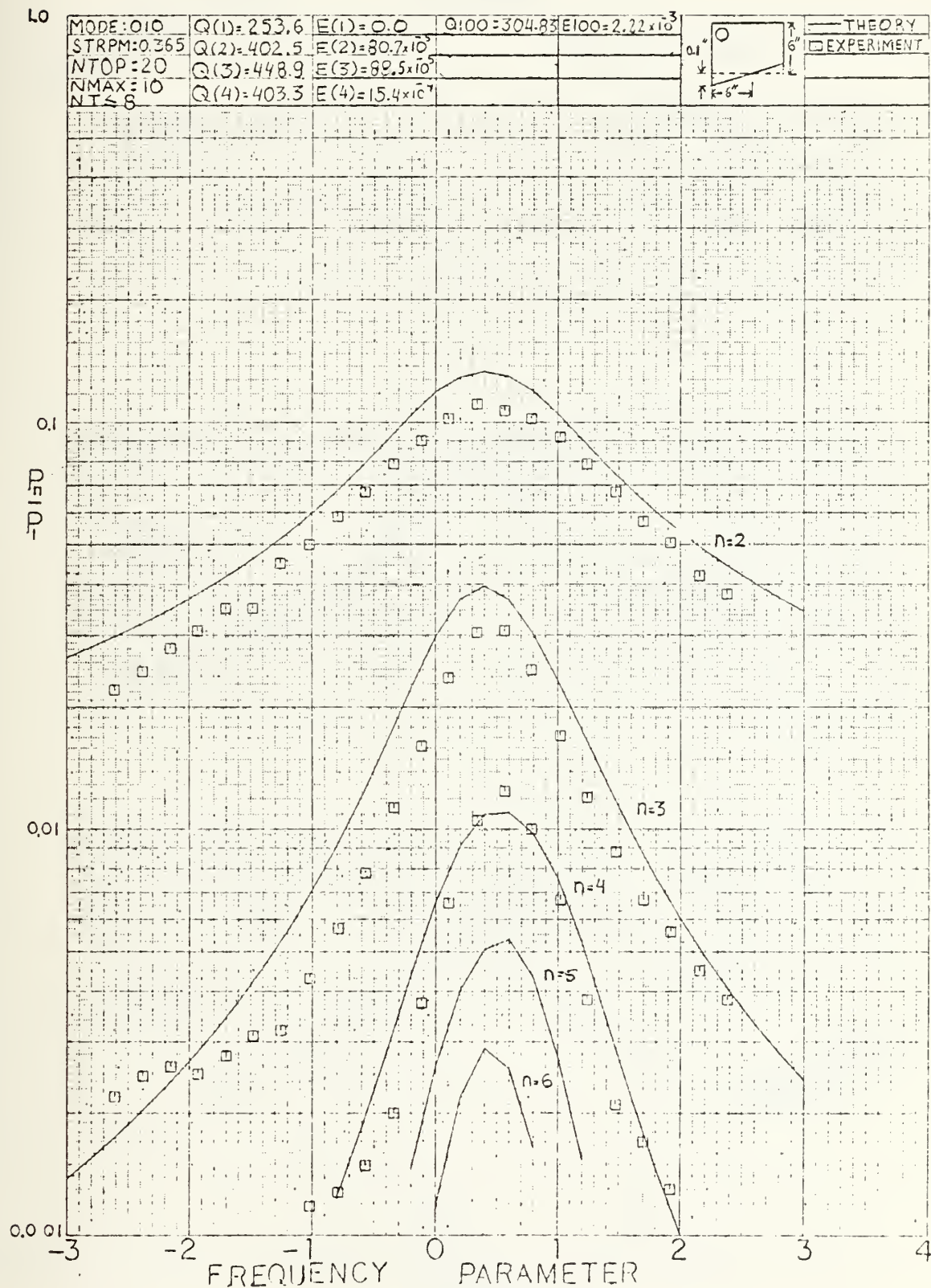


FIGURE 9



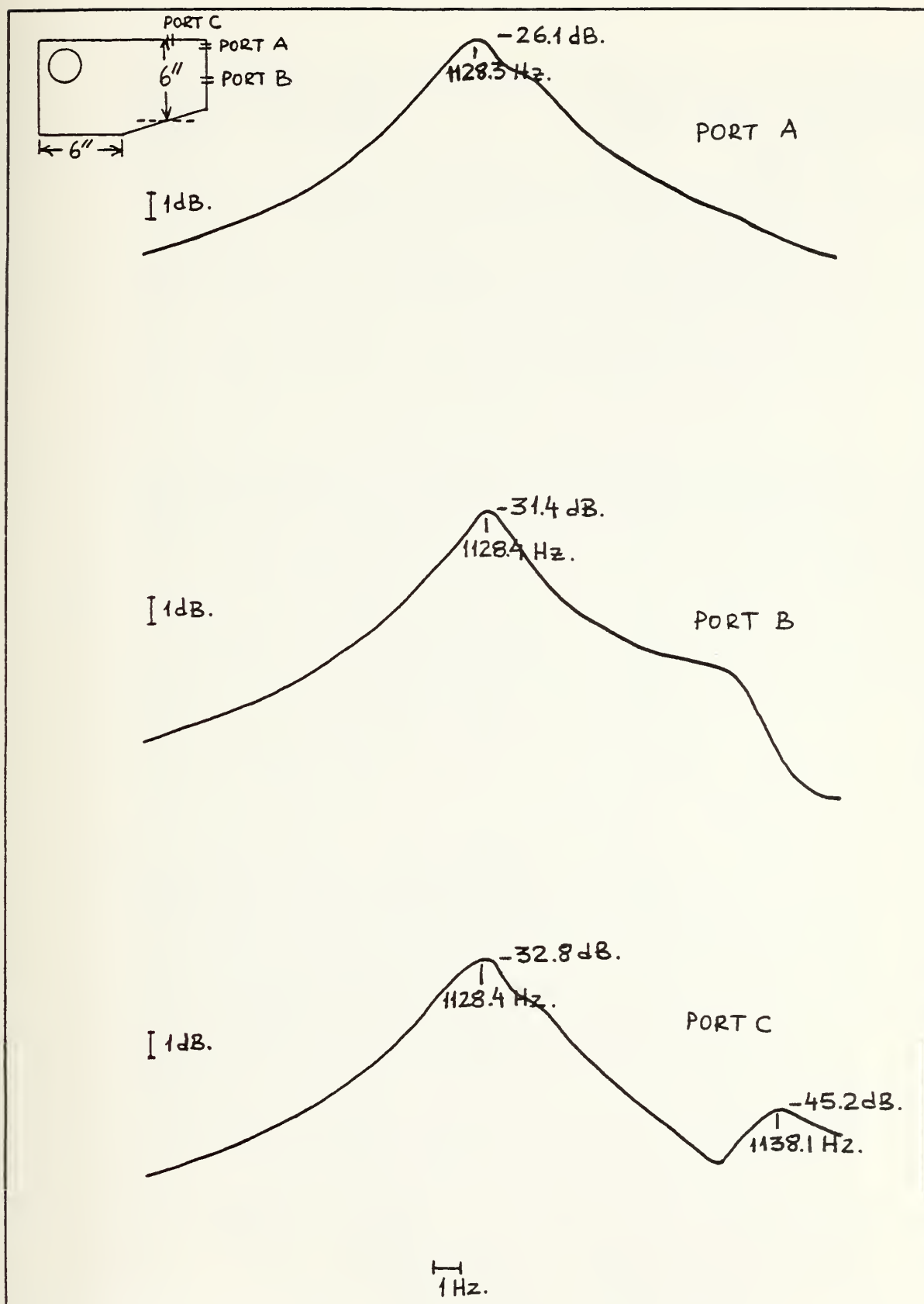


FIGURE 10



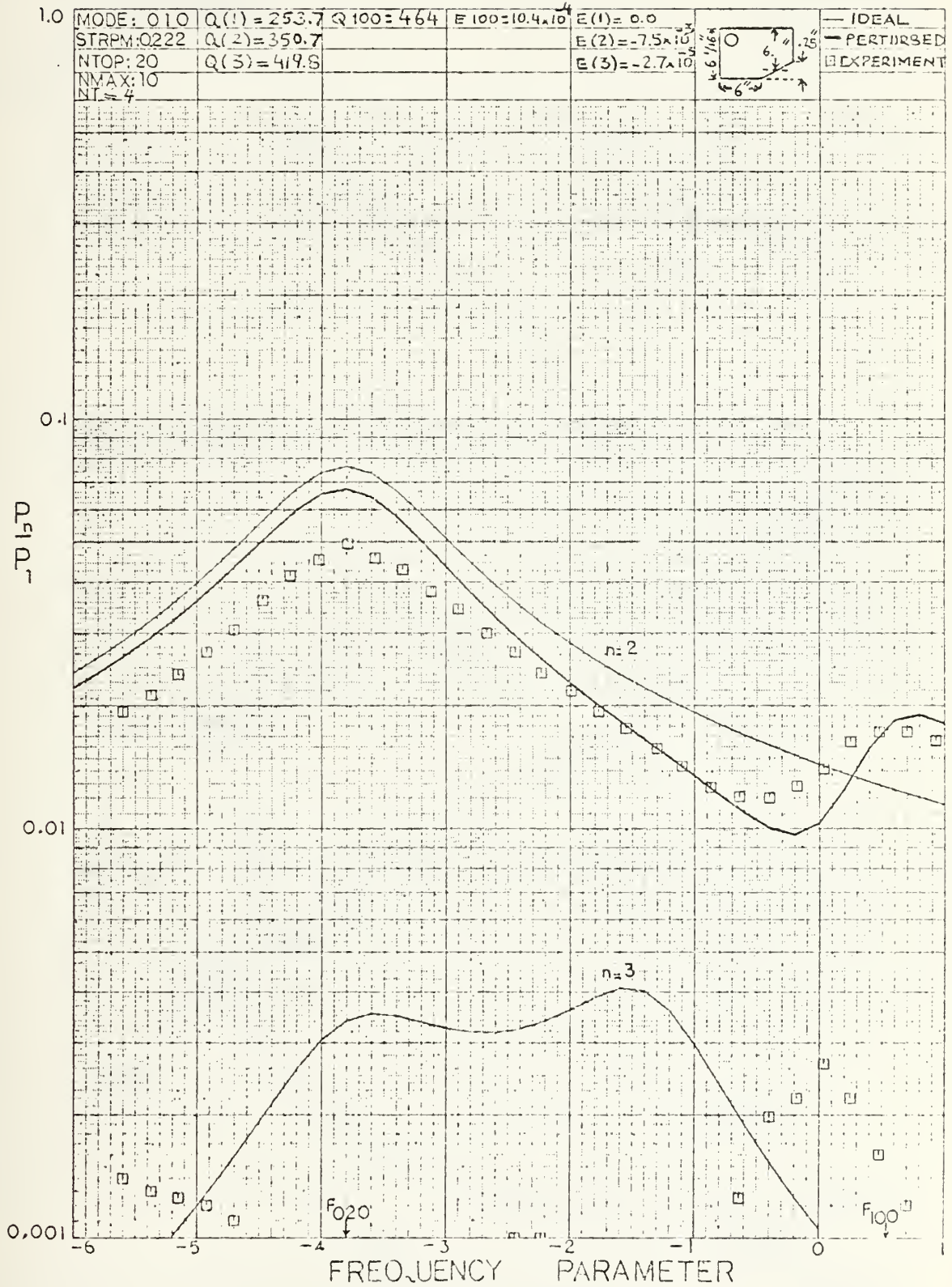


FIGURE 11

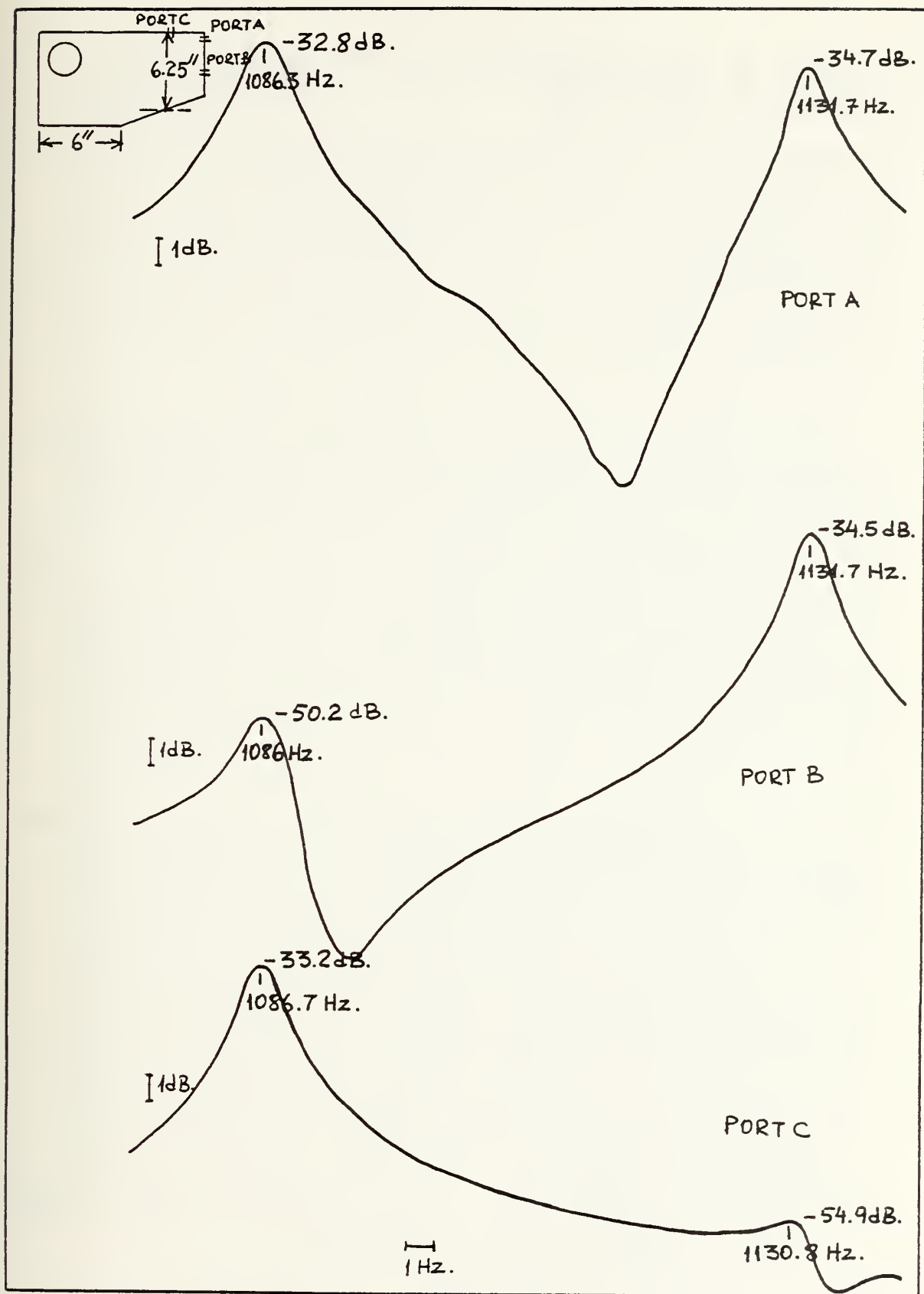


FIGURE 12

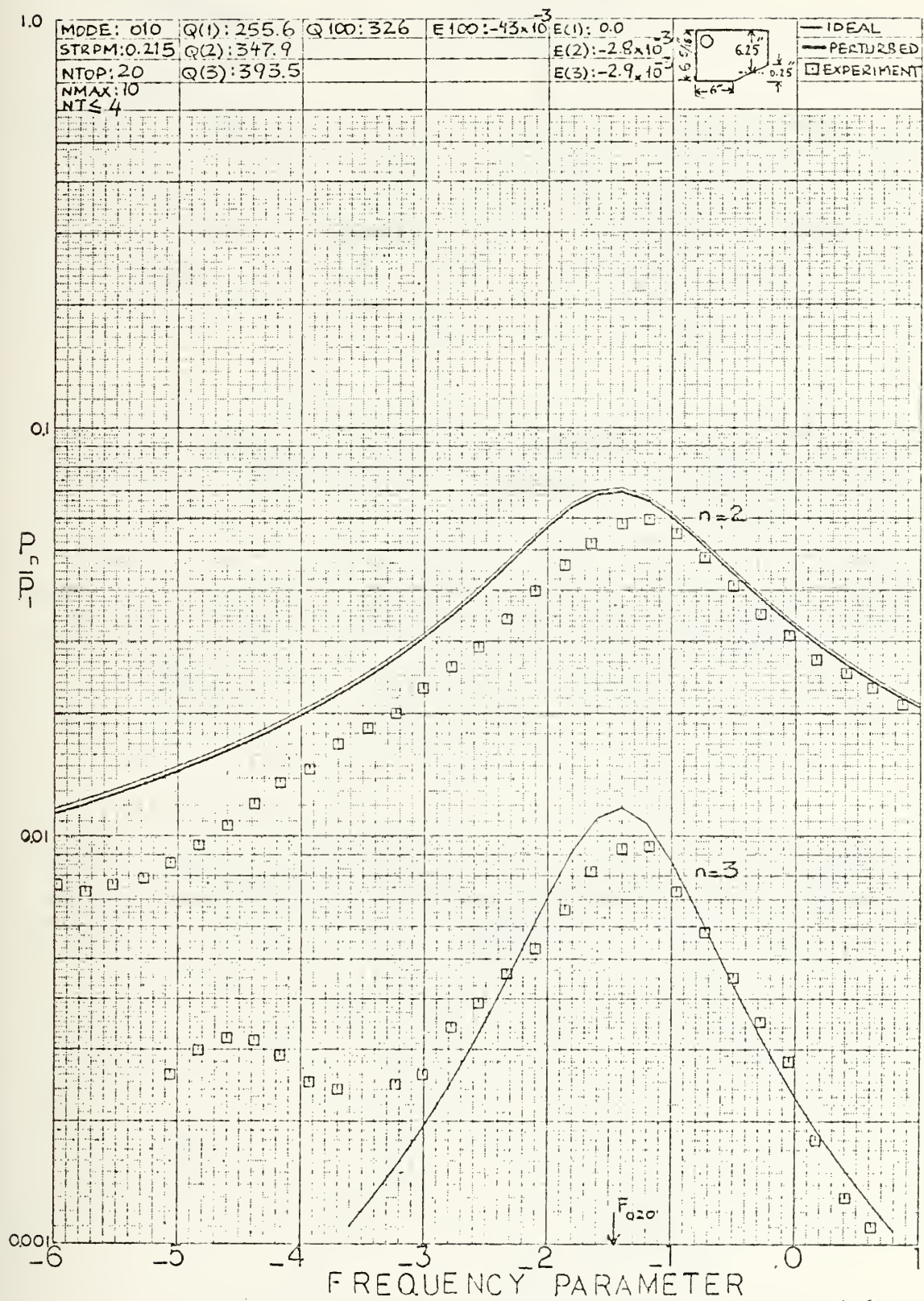


FIGURE 13

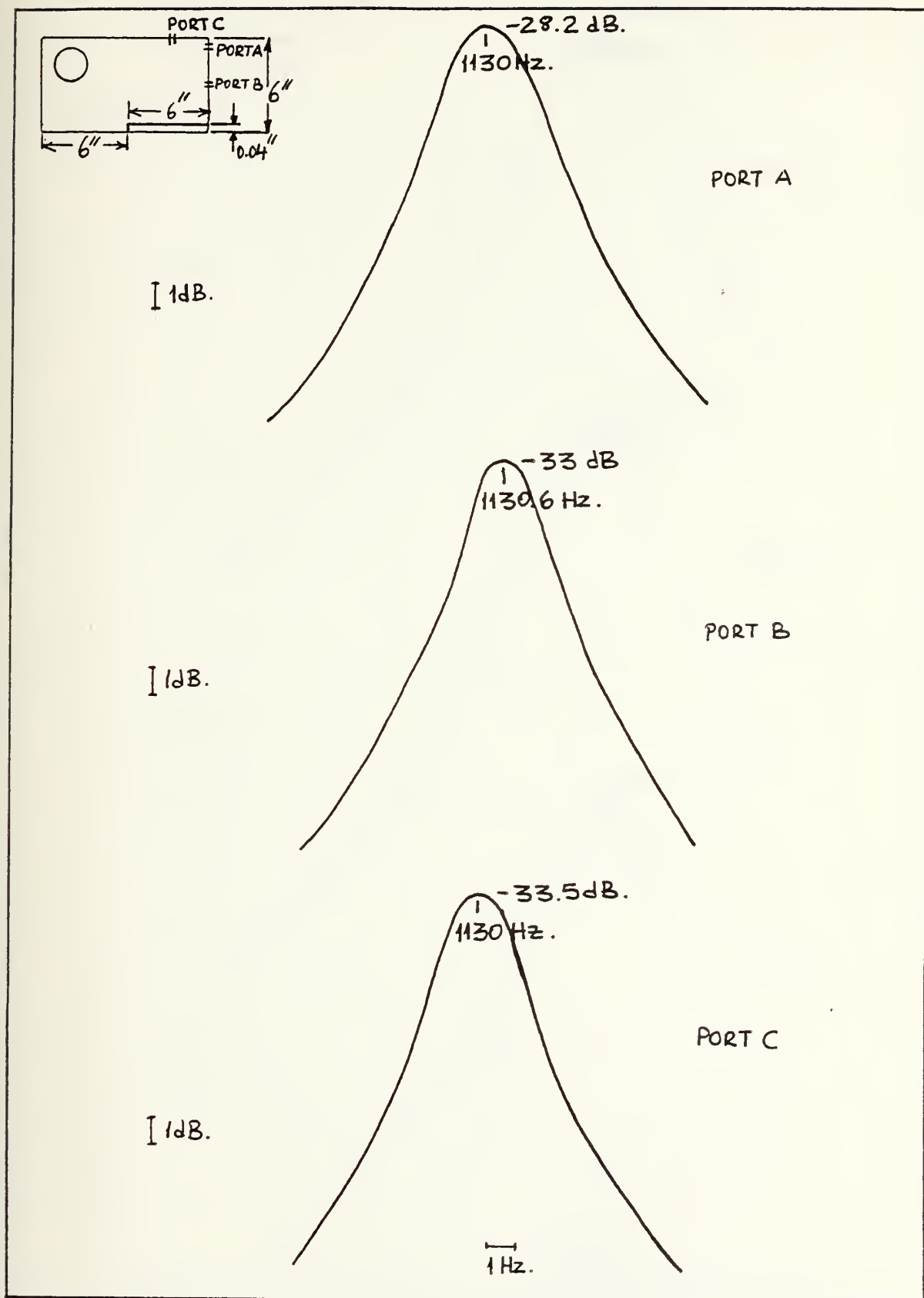


FIGURE 14

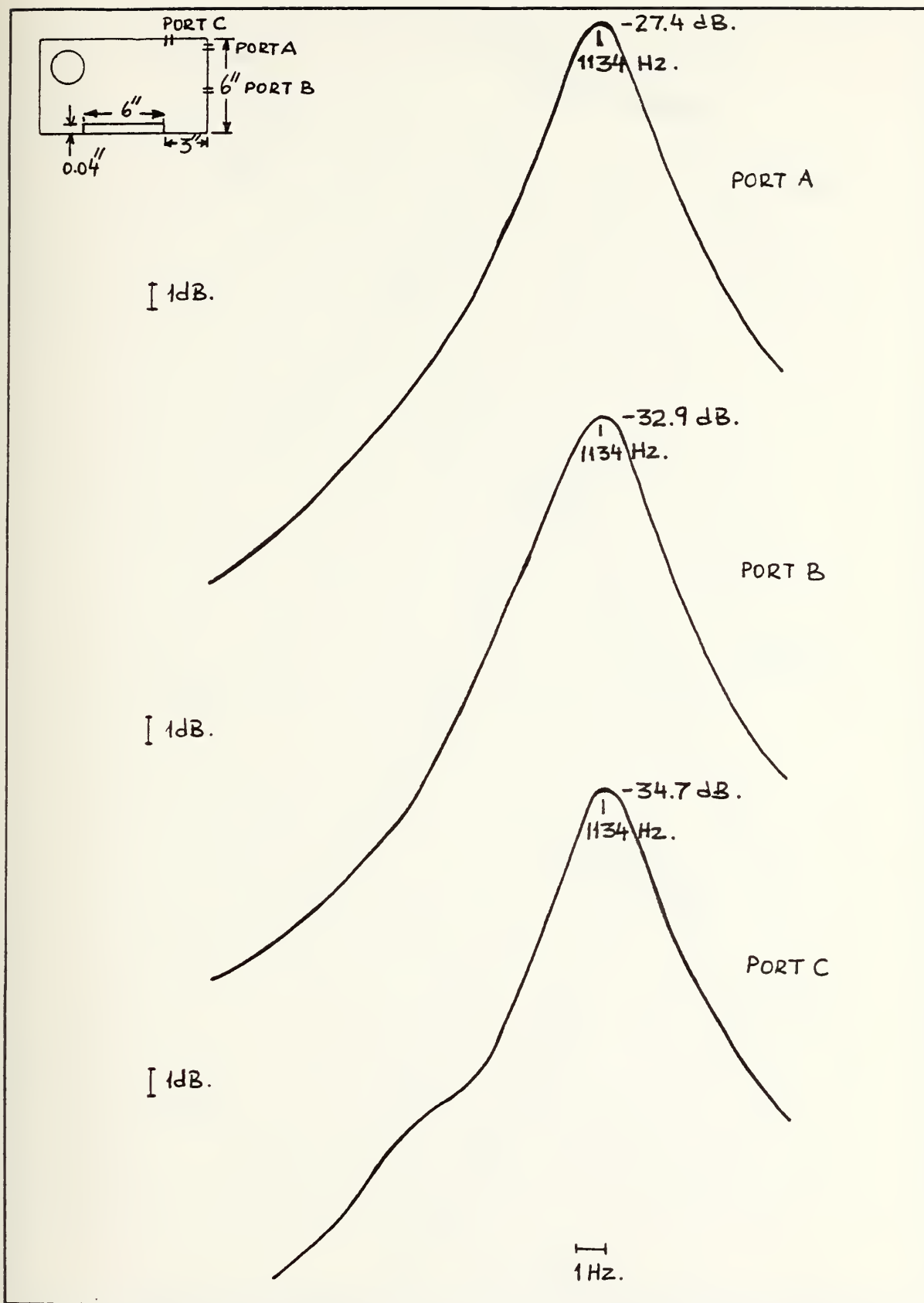


FIGURE 15

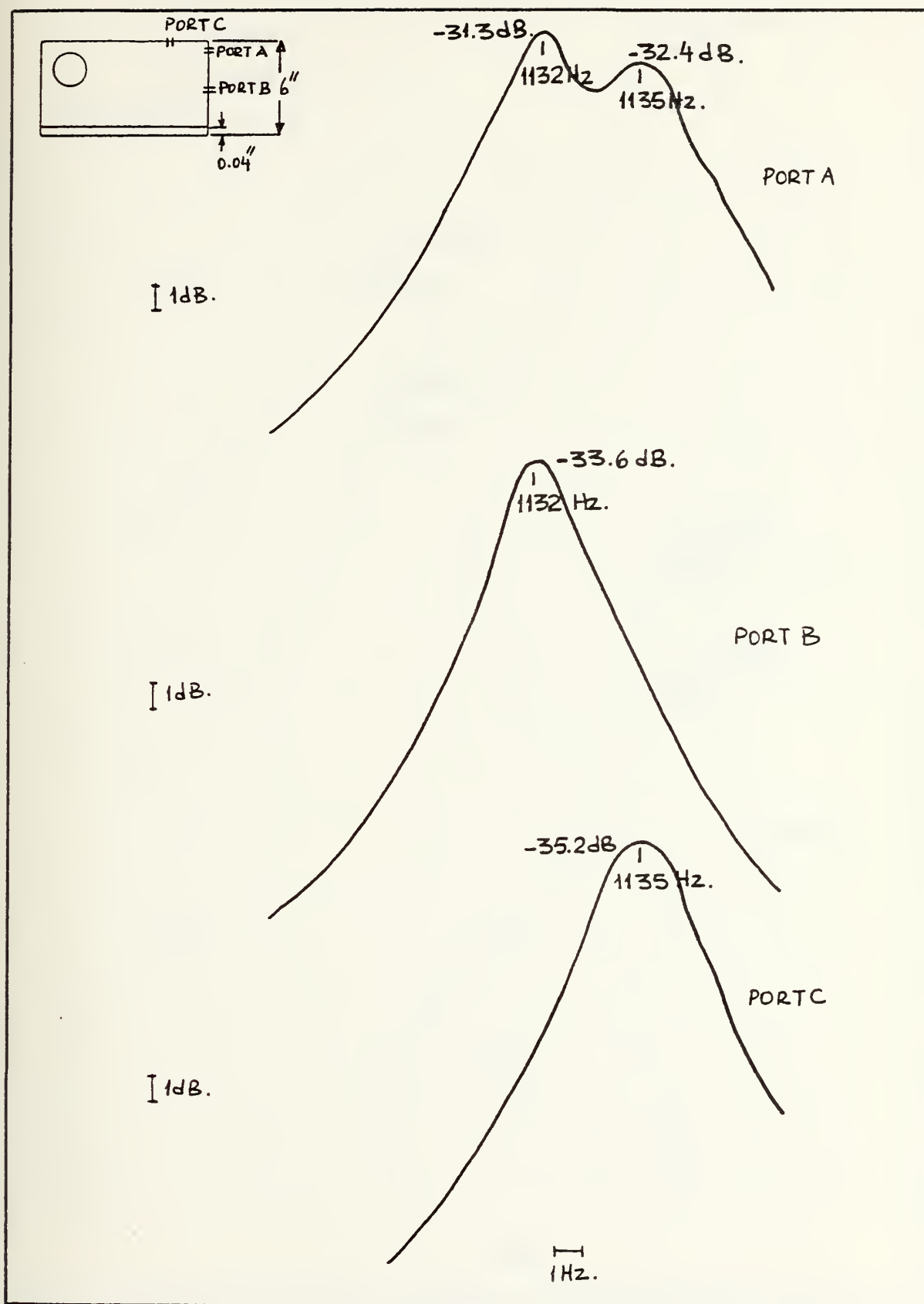


FIGURE 16

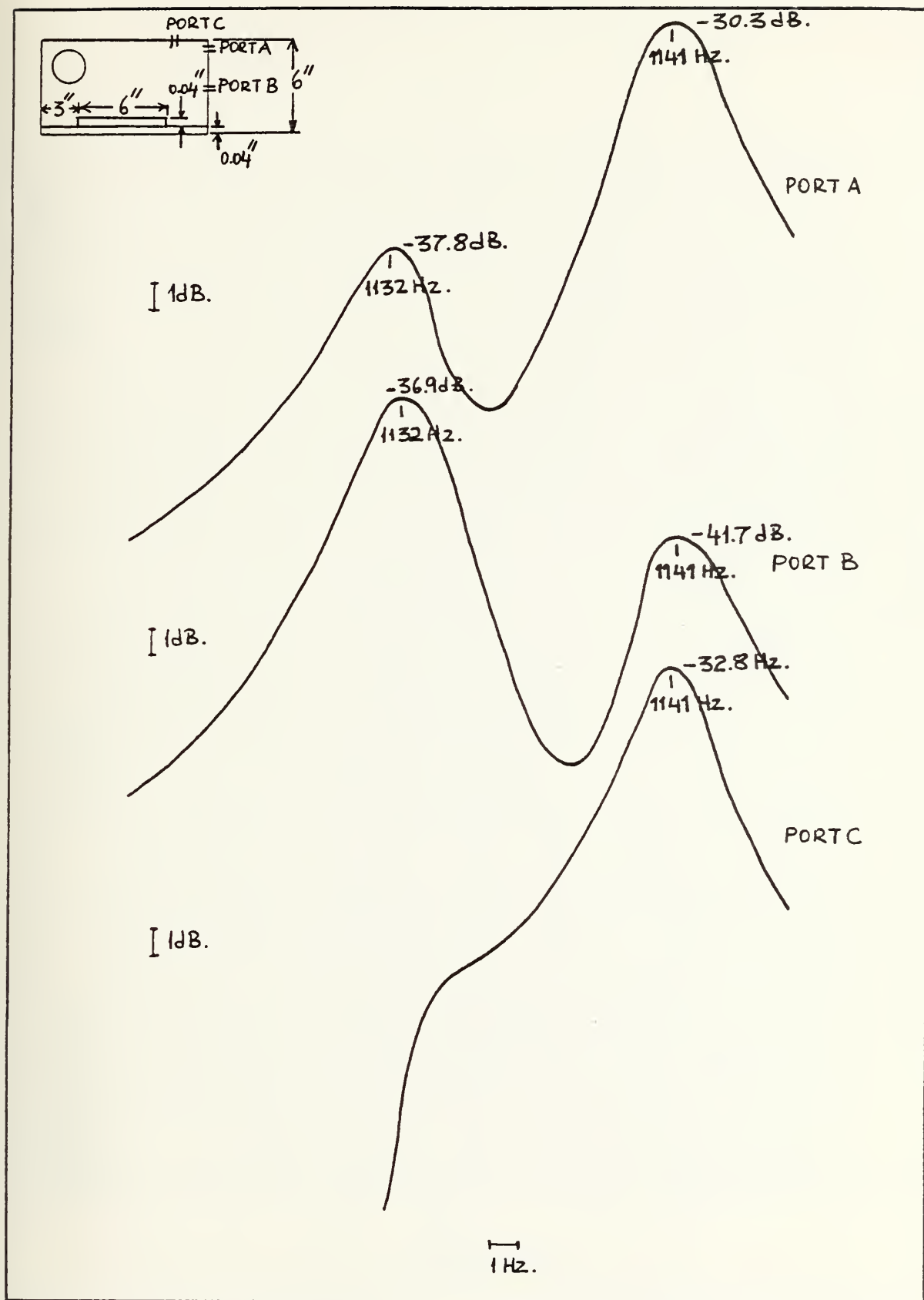
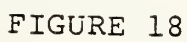


FIGURE 17



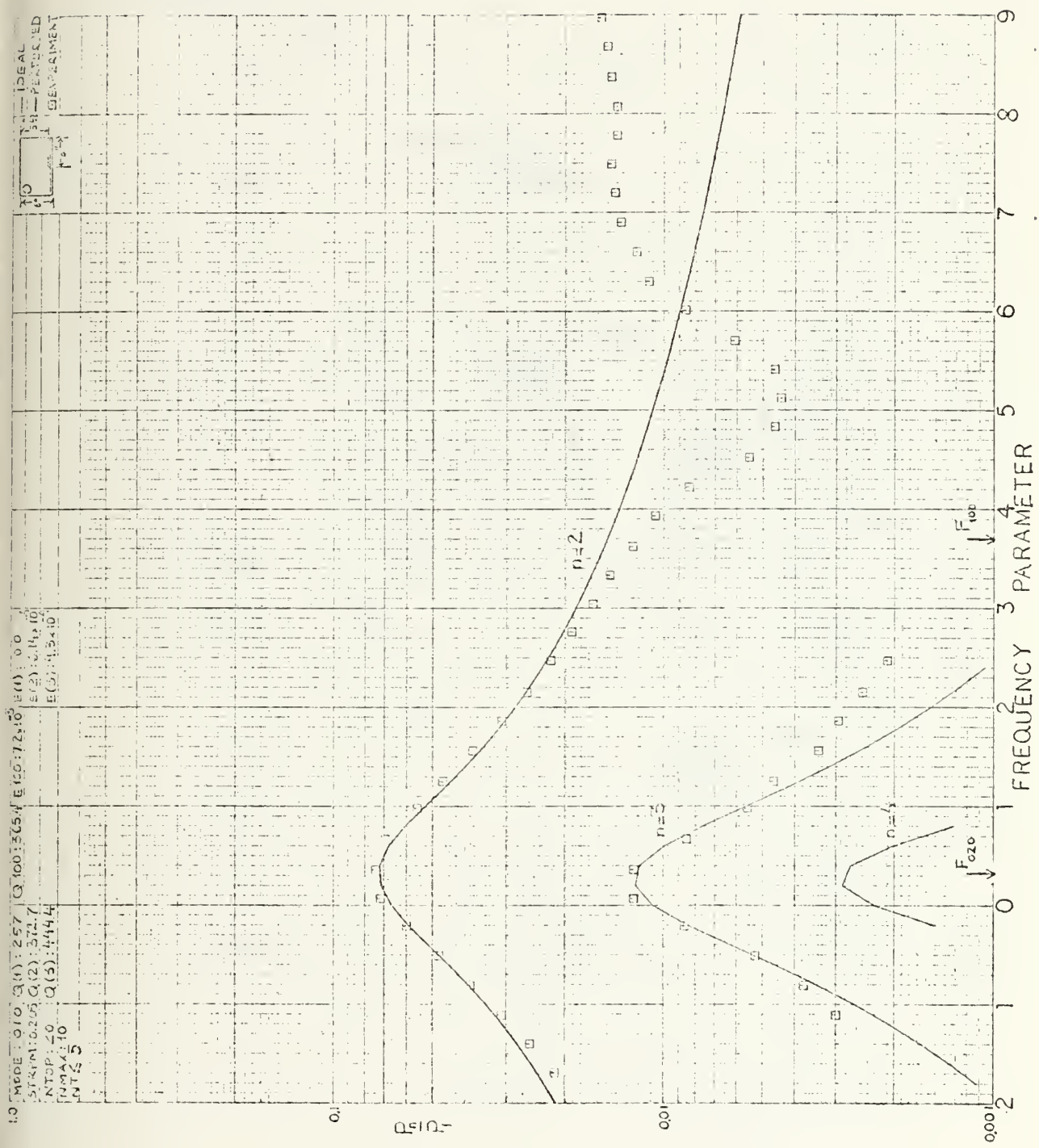


FIGURE 19

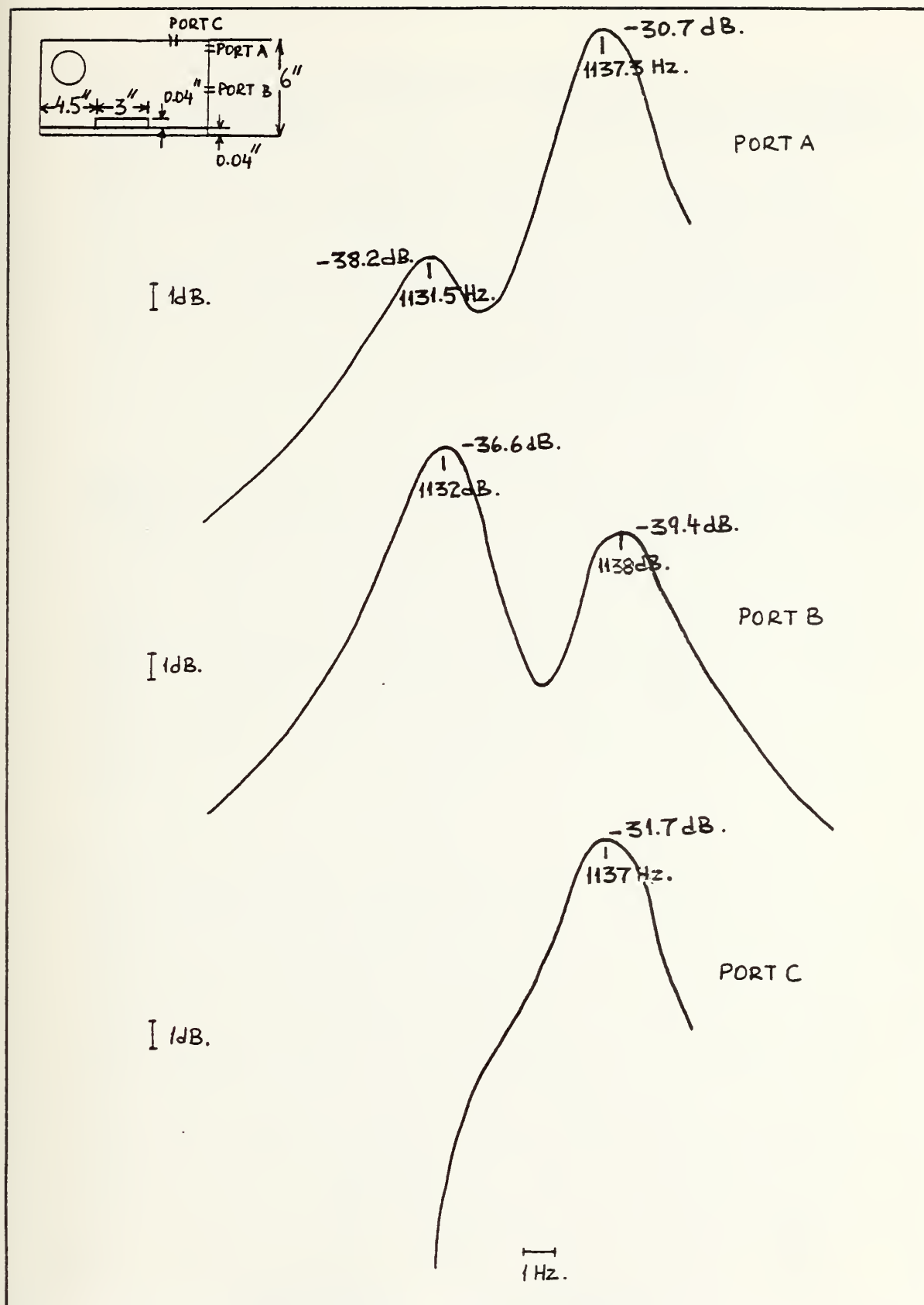


FIGURE 20

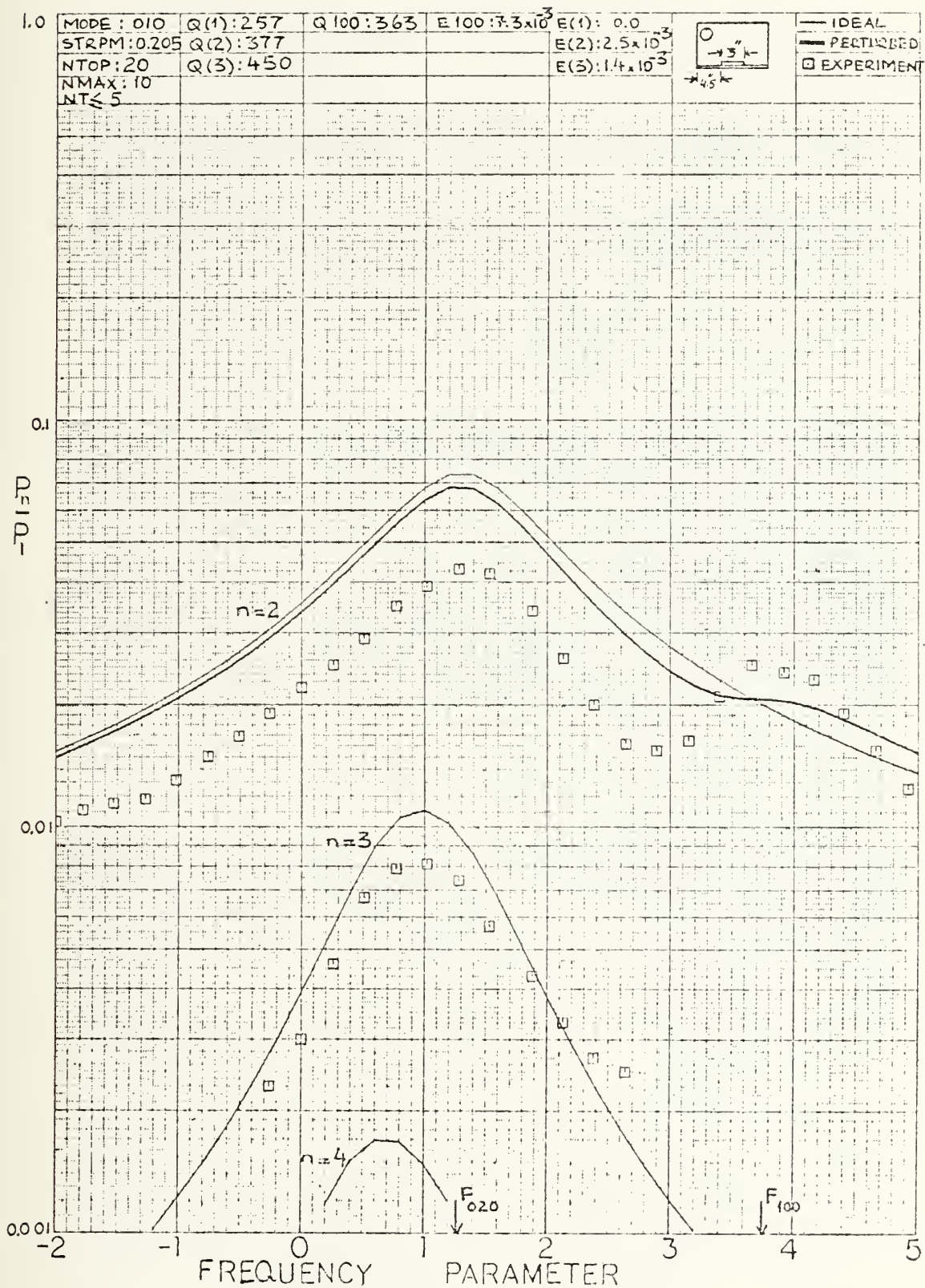


FIGURE 21

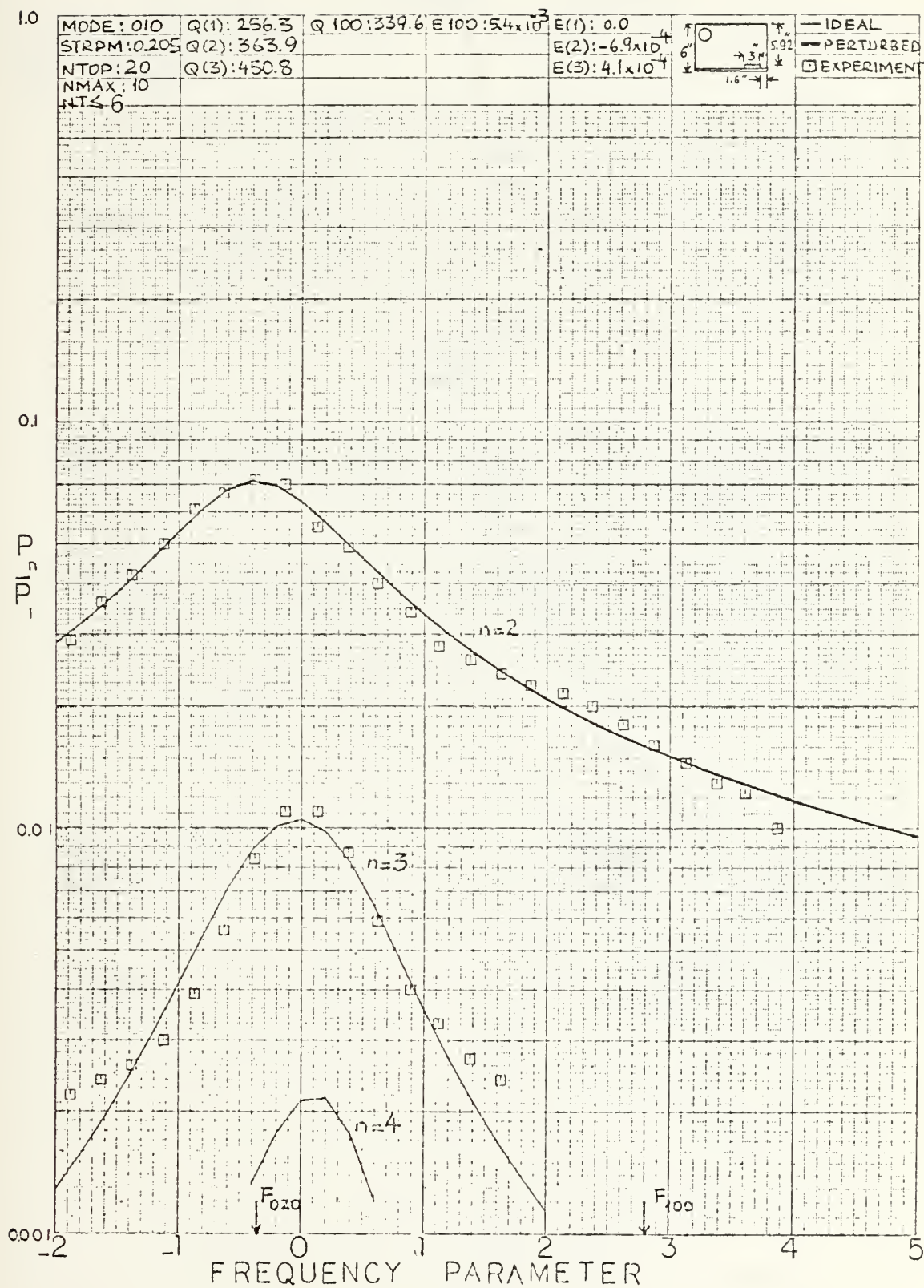


FIGURE 22

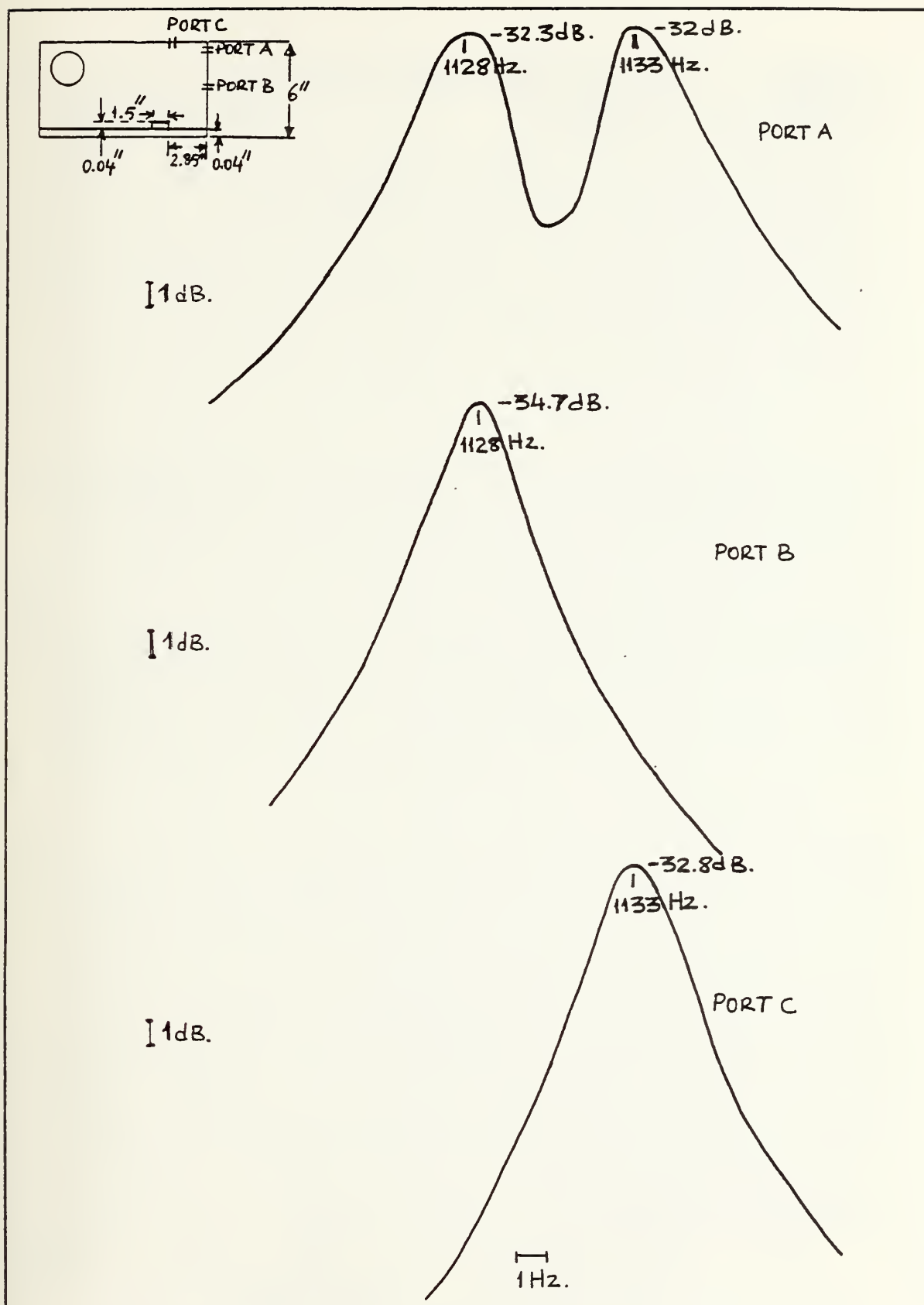


FIGURE 23

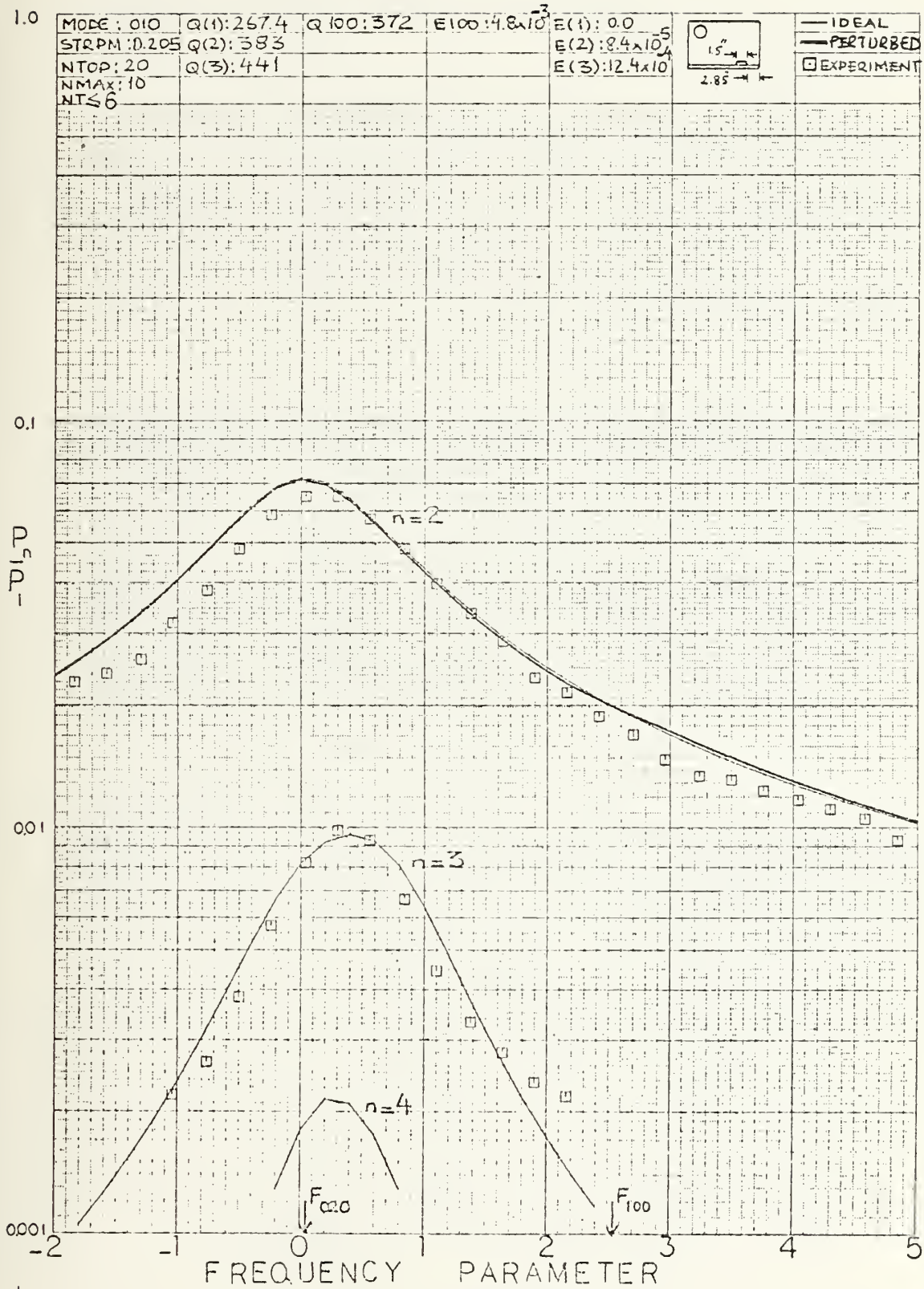


FIGURE 24

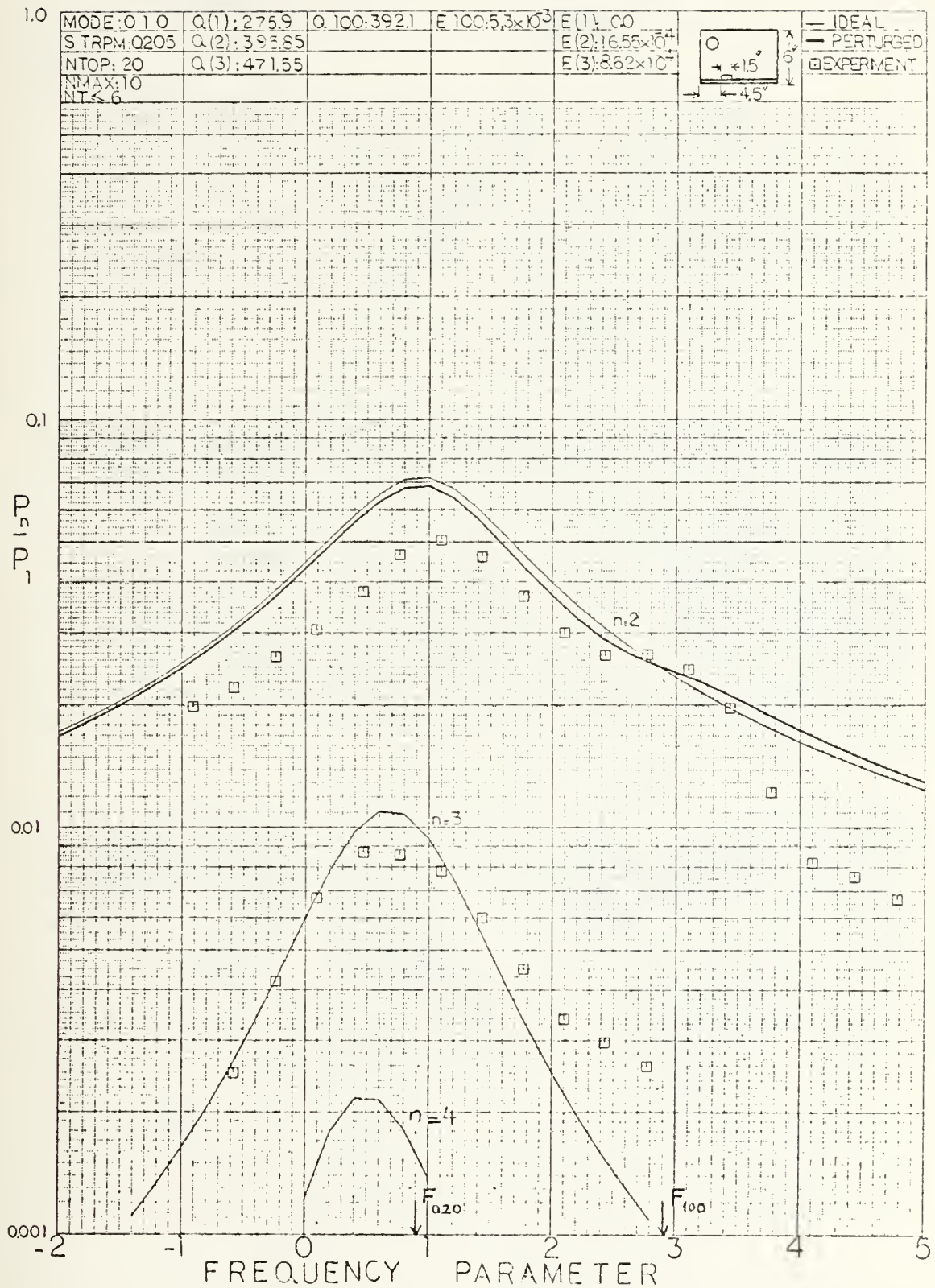


FIGURE 25

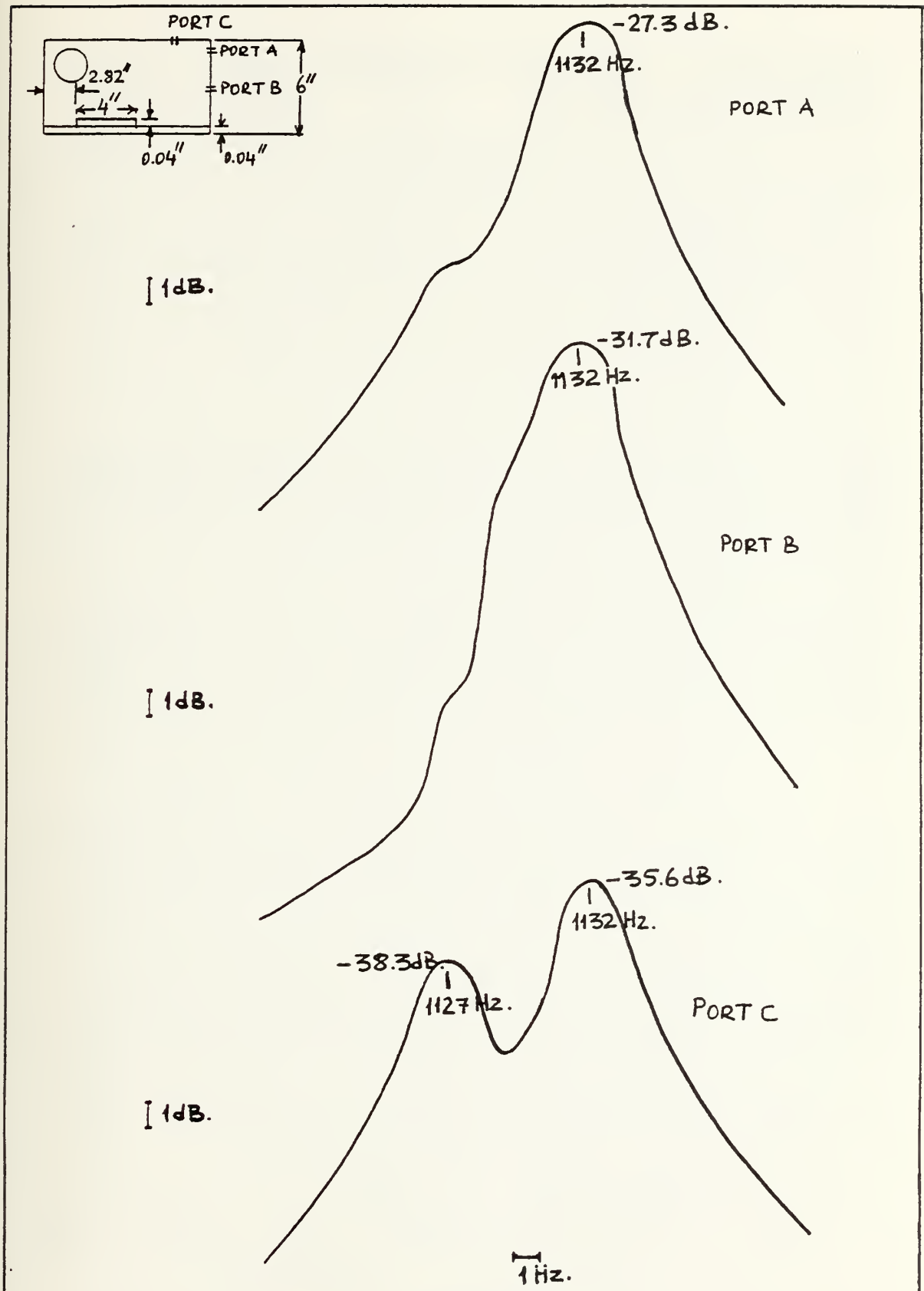


FIGURE 26

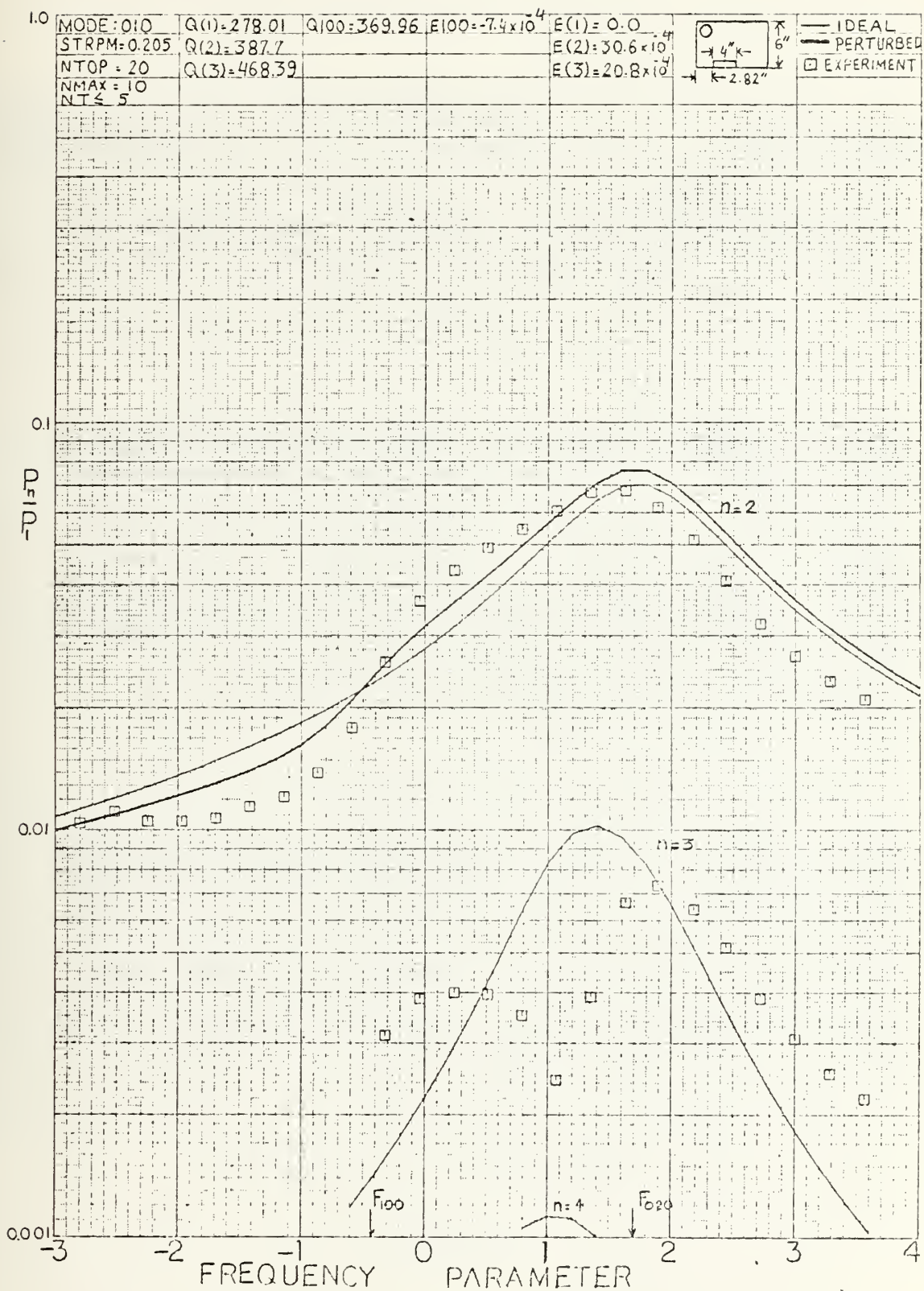


FIGURE 27

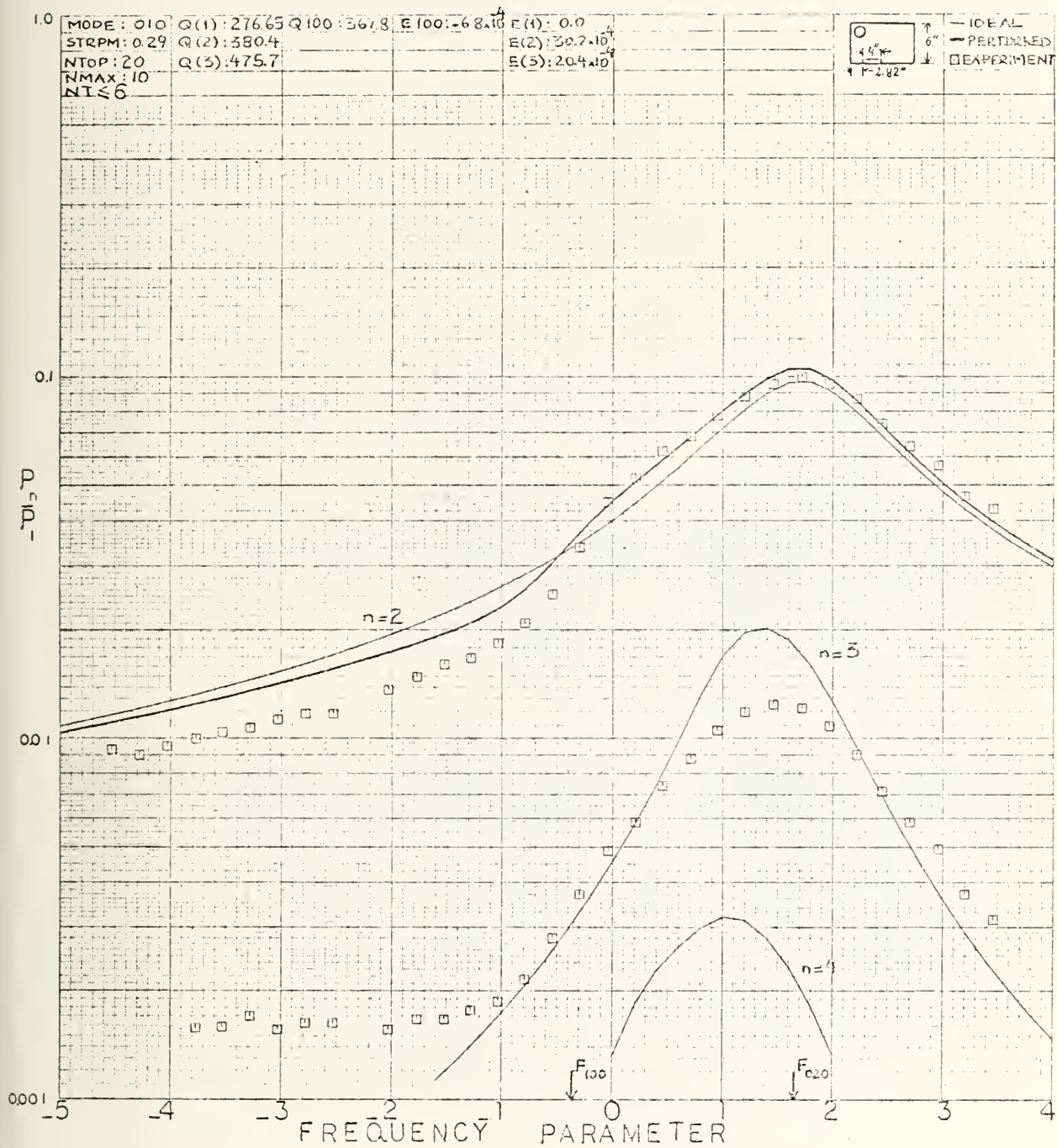


FIGURE 28

APPENDIX B

TABLES

CONFIGURATION	MODE					
	010	100	020	110	120	030
12" x 5.5" x 2.5"	565	1234	1131	1358	1674	1697
12" x 7.75" x 2.5"	565	1181	1131	1309	1635	1697
12" x 6.0" x 2.5"	565	1131	1131	1265	1600	1697
12" x 6.25" x 2.5"	565	1086	1131	1224	1568	1697
12" x 6.5" x 2.5"	565	1039	1131	1183	1536	1697
12" x 6.75" x 2.5"	565	1008	1131	1156	1515	1697
12" x 7.0" x 2.5"	565	970	1131	1123	1490	1697

TABLE I. THEORETICALLY PREDICTED MODES

TABLE II
(See Fig. 8)

PRE-RUN

n	t(min.)	f_u	f_L	f_r	Q	E
010	0	566.28	564.08	565.18	256.9	0
020	7	1132.78	1129.89	1131.335	391.46	76.63×10^{-5}
030	8	1698.86	1695.2	1697.03	463.67	75.5×10^{-5}
040	11	2266.18	2261.88	2264.03	526.52	12.69×10^{-4}
100	4	1128.18	1125.07	1126.625	362.25	33.57×10^{-4}

FINITE-AMPLITUDE RUN

t(min.)	f(Hz)	V_2 (dB)	V_3 (dB)	V_4 (dB)	V_2/V_1	V_3/V_1	V_4/V_1	FP
16	563.3	-21.5	-42.7	-	0.0382	0.0033	-	-1.86
21	563.6	-20.6	-41.3	-	0.0424	0.0039	-	-1.64
26	563.9	-19.2	-39.7	-54.5	0.0498	0.0047	0.00085	-1.42
31	564.2	-18.6	-38.1	-52.2	0.0534	0.0056	0.0011	-1.19
36	564.5	-17.8	-36.1	-50.1	0.0585	0.007	0.0014	-0.97
41	564.8	-16.5	-33.8	-47.3	0.068	0.0093	0.0019	-0.74
46	565.1	-15.4	-31.5	-43.2	0.077	0.012	0.003	-0.52
51	565.4	-14	-27.7	-39.1	0.09	0.018	0.005	-0.29
56	565.7	-12.7	-24.7	-34.8	0.105	0.026	0.0083	-0.07
61	566.0	-12	-22	-31.9	0.114	0.036	0.0115	0.16
66	566.3	-11.5	-20.7	-30	0.12	0.0419	0.014	0.38
71	566.6	-11.9	-21.3	-29.8	0.1150	0.039	0.014	0.62
76	566.9	-12.8	-23.1	-31.4	0.1040	0.032	0.012	0.83
81	567.2	-14	-25.5	-34.6	0.09	0.024	0.008	1.06
86	567.5	-15.5	-28.4	-38.6	0.0760	0.018	0.0053	1.28
91	567.8	-16.5	-31.5	-42.5	0.068	0.012	0.0034	1.5
96	568.1	-17.4	-34.2	-46.8	0.0613	0.088	0.0021	1.74
101	568.4	-18.4	-36.9	-50	0.055	0.0065	0.0014	2.00
105	568.7	-19	-38.1	-53	0.051	0.0056	0.001	2.18

POST-RUN

n	t(min.)	f_u	f_L	f_r	Q	E
010	113	567.48	565.3	566.39	259.81	0
020	118	1135.28	1132.38	1133.83	390.97	83.86×10^{-5}
030	114	1702.49	1698.65	1700.57	442.85	82.39×10^{-5}
040	117	2271.0	2266.6	2268.8	515.64	13.59×10^{-4}
100	120	1130.79	1127.58	1129.18	351.77	-32.97×10^{-4}

AVERAGE VALUES OF Q'S AND E'S

n	Q	E
010	258.36	0
020	391.22	79.745×10^{-5}
030	453.26	78.935×10^{-5}
040	521.08	13.142×10^{-4}
100	357	-33.27×10^{-4}

TABLE III
(See Fig. 9)

PRE-RUN

n	t(min.)	f_u	f_L	f_r	Q	E
010	0	567.08	564.89	565.985	258.44	0
020	4	1134.3	1131.56	1132.93	413.47	78.62×10^{-5}
030	6	1701.68	1697.9	1699.79	449.68	98.34×10^{-5}
040	10	2270.96	2265.3	2268.13	400.72	170.03×10^{-5}
100	13	1136.75	1132.67	1134.71	278.12	221.7×10^{-5}

FINITE AMPLITUDE RUN

t(min.)	f(Hz)	V_2 (dB)	V_3 (dB)	V_4 (dB)	V_2/V_1	V_3/V_1	V_4/V_1	FP
21	563.0	-26.4	-48.4	-	0.0239	0.0019	-	-2.84
26	563.3	-27.1	-47	-	0.022	0.0022	-	-2.61
31	563.6	-26.2	-46.1	-	0.0244	0.00247	-	-2.38
36	563.9	-25.1	-45.7	-	0.0278	0.0026	-	-2.15
41	564.2	-24.2	-45.8	-	0.031	0.0025	-	-1.93
46	564.5	-23.1	-45.1	-	0.035	0.0027	-	-1.7
51	564.8	-23.1	-44.1	-	0.035	0.0031	-	-1.48
56	565.1	-20.9	-43.9	-	0.045	0.0032	-	-1.255
61	565.4	-19.9	-41.3	-52.5	0.05	0.0043	0.00118	-1.02
66	565.7	-18.6	-38.8	-51.8	0.0587	0.0057	0.00128	-0.79
71	566.0	-17.4	-36.1	-50.5	0.067	0.0078	0.00149	-0.57
76	566.3	-16	-32.9	-47.1	0.079	0.0113	0.002	-0.34
81	566.6	-14.9	-29.6	-42.5	0.089	0.016	0.00374	-0.116
86	566.9	-13.8	-26.5	-37.6	0.102	0.0236	0.00659	0.107
91	567.2	-13.1	-24.3	-33.5	0.11	0.0304	0.0105	0.34
96	567.5	-13.4	-24.1	-32.1	0.107	0.0308	0.0124	0.56
101	567.8	-13.8	-26.1	-33.7	0.102	0.0247	0.001	0.787
106	568.1	-14.7	-29.1	-37.4	0.092	0.017	0.0067	1.019
111	568.4	-16	-32.3	-42.3	0.079	0.012	0.0038	1.24
116	568.7	-17.4	-35	-47.4	0.067	0.0088	0.0021	1.48
121	569.0	-18.8	-37.4	-49.1	0.057	0.0067	0.0017	1.699
126	569.3	-19.9	-39	-51.6	0.05	0.0056	0.0013	1.92
131	569.6	-21.4	-40.9	-	0.042	0.0045	-	2.155
136	569.9	-22.4	-42.3	-	0.038	0.0038	-	2.378

POST-RUN

n	t(min.)	f_u	f_L	f_r	Q	E
010	134	568.37	566.09	567.23	248.78	0
020	142	1136.85	1133.95	1135.4	391.51	82.86×10^{-5}
030	138	1705.05	1701.25	1703.15	448.51	78.74×10^{-5}
040	140	2275.1	2269.5	2272.3	405.76	138.4×10^{-5}
100	145	1138.9	1135.47	1137.185	331.54	222.53×10^{-5}

TABLE III (Cont.)

AVERAGE VALUES OF Q'S AND E'S

n	Q	E
010	253.61	0
020	402.49	80.74×10^{-5}
030	448.935	88.54×10^{-5}
040	403.24	154.215×10^{-5}
100	304.83	222.115×10^{-5}

TABLE IV
(See Fig. 11)

PRE-RUN

n	t	f_u	f_L	f_r	Q	E
010	0	567.3	565.05	566.175	251.6	0
020	5	1125.4	1122.18	1123.79	349.0	-7.39×10^{-3}
030	2	1695.76	1691.57	1693.67	404.2	-2.6×10^{-3}
100	7	1134.8	1134.27	1136.0	460.0	10.8×10^{-4}

FINITE-AMPLITUDE RUN

t (min.)	f (Hz)	V_2 (dB)	V_1 (dB)	V_2/V_1	V_3/V_1	FP
15	560.0	-32.4	-55.2	0.0193	0.0014	-5.6
18	560.3	-31.6	-55.5	0.0212	0.0013	-5.37
21	560.6	-30.6	-56.2	0.0238	0.00125	-5.15
24	560.9	-29.5	-56.5	0.027	0.0012	-4.92
27	561.2	-28.4	-57.2	0.0306	0.0011	-4.7
30	561.5	-27.0	-	0.036	-	-4.47
33	561.8	-25.8	-	0.0414	-	-4.25
36	562.1	-25.0	-	0.0453	-	-4.02
39	562.4	-24.7	-	0.0469	-	-3.79
42	562.7	-24.9	-	0.0458	-	-3.57
45	563.0	-25.5	-	0.0428	-	-3.35
48	563.3	-26.4	-	0.038	-	-3.12
51	563.6	-27.4	-	0.0344	-	-2.9
54	563.9	-28.5	-	0.03	-	-2.67
57	564.2	-29.5	-58.1	0.027	0.001	-2.44
60	564.5	-30.4	-57.5	0.024	0.001	-2.23
63	564.8	-31.4	-	0.0217	-	-1.99
66	565.1	-32.4	-	0.0193	-	-1.77
69	565.4	-33.2	-	0.0176	-	-1.55
72	565.7	-34.2	-	0.0157	-	-1.3
75	566.0	-35.1	-	0.0142	-	-1.1
78	566.3	-36.1	-	0.0126	-	-0.87
81	566.6	-36.5	-56.2	0.012	0.00125	-0.64
84	566.9	-36.6	-52.2	0.0119	0.00198	-0.4
87	567.2	-36.0	-51.1	0.0127	0.0022	-0.18
90	567.5	-35.0	-49.6	0.014	0.00267	0.035
93	567.8	-33.9	-50.9	0.0163	0.0022	0.25
96	568.1	-33.4	-53.6	0.0172	0.0016	0.48
99	568.4	-33.4	-56.5	0.0172	0.0012	0.7
102	568.7	-33.8	-	0.0164	-	0.93
105	569.0	-34.1	-	0.0159	-	1.16
108	569.3	-34.6	-	0.015	-	1.38
111	569.6	-35.1	-	0.0142	-	1.6
114	569.9	-35.6	-	0.0133	-	1.83
117	570.2	-36.1	-	0.0126	-	2.03
120	570.5	-36.6	-	0.0119	-	2.28
123	570.8	-37.2	-	0.0111	-	2.5
126	571.1	-38.0	-	0.0101	-	2.72

TABLE IV (Cont.)

POST-RUN

n	t (min.)	f_u	f_L	f_r	Q	E
010	121	569.07	566.85	567.96	255.8	0
020	127	1129.08	1125.88	1127.48	352.34	-7.6×10^{-3}
030	118	1700.95	1697.05	1699.	435.64	-2.79×10^{-3}
100	128	1138.36	1135.93	1137.1	468.	10×10^{-4}

AVERAGE VALUES OF Q'S AND E'S

n	Q	E
010	253.7	0
020	350.7	-7.495×10^{-3}
030	419.8	-2.695×10^{-3}
100	464	10.4×10^{-4}

TABLE V
(See Fig. 13)

PRE-RUN

n	t(min.)	f_u	f_L	f_r	Q	E
010	0	568.6	566.37	567.485	254.47	0
020	6	1133.18	1130.25	1131.72	386.25	-2.99×10^{-3}
030	3	1699.75	1696	1697.875	452.76	-2.7×10^{-3}
100	9	1088.5	1085.15	1086.3	324.3	-43.34×10^{-3}

FINITE-AMPLITUDE RUN

t (min.)	f(Hz)	V_2 (dB)	V_3 (dB)	V_2/V_1	V_3/V_1	PP
46	560.	-44.1	-51.1	0.005	-	-7.35
49	560.3	-43.5	-51.5	0.0055	-	-7.12
52	560.6	-43.1	-	0.0058	-	-6.88
55	560.9	-42.1	-51.4	0.0065	-	-6.7
58	561.2	-42.1	-	-	-	-6.43
61	561.5	-41.5	-	0.007	-	-6.2
64	561.8	-40.8	-	0.0076	-	-5.98
67	562.1	-41.1	-	0.0073	-	-5.75
70	562.4	-40.8	-	0.0076	-	-5.53
73	562.7	-40.4	-	0.0079	-	-5.28
76	563.0	-39.7	-50.0	0.0086	0.0026	-5.06
79	563.3	-38.8	-48.9	0.0095	0.00299	-4.83
82	563.6	-37.9	-48.2	0.0106	0.0032	-4.6
85	563.9	-36.9	-48.4	0.012	0.00316	-4.38
88	564.2	-35.8	-49.1	0.0135	0.0029	-4.17
91	564.5	-35.1	-50.3	0.0146	0.0025	-3.93
94	564.8	-33.9	-50.8	0.0168	0.0024	-3.7
97	565.1	-33.1	-	0.0184	-	-3.46
100	565.4	-32.1	-50.6	0.02	0.00246	-3.23
103	565.7	-31.2	-50.2	0.023	0.0026	-3.01
106	566.0	-30.1	-47.6	0.026	0.0034	-2.78
109	566.3	-29	-46.6	0.029	0.0039	-2.56
112	566.6	-27.8	-45.1	0.034	0.0046	-2.33
115	566.9	-26.4	-43.8	0.0398	0.0053	-2.1
118	567.2	-25.1	-42.	0.046	0.0066	-1.86
121	567.5	-24	-40.1	0.052	0.0082	-1.65
124	567.8	-23.1	-39.0	0.058	0.0093	-1.4
127	568.1	-22.9	-38.9	0.0596	0.00945	-1.18
130	568.4	-23.6	-41.1	0.055	0.0073	-0.96
133	568.7	-24.8	-43.1	0.048	0.0058	-0.73
136	569.0	-26.1	-45.2	0.041	0.0045	-0.5
139	569.3	-27.3	-47.3	0.035	0.0035	-0.28
142	569.6	-28.5	-49.5	0.031	0.0028	-0.05
145	569.9	-29.6	-53.1	0.027	0.0018	0.17
148	570.2	-30.5	-55.7	0.025	0.0013	0.41
151	570.5	-31.2	-57.1	0.023	0.0011	0.62
154	570.8	-31.9	-	0.021	-	0.86
157	571.1	-33.0	-	0.018	-	1.09
160	571.4	-33.7	-	0.016	-	1.3

TABLE V (Cont.)

n	t(min.)	f_u	f_L	f_r	Q	E
010	149	570.87	568.65	569.76	256.65	0
020	151	1138.05	1134.38	1136.215	309.6	-2.69×10^{-3}
030	150	1707.2	1702.1	1704.65	334.25	-2.74×10^{-3}
100	161	1091.7	1088.35	1089.5	328.6	-44×10^{-3}

AVERAGE VALUES OF Q'S AND E'S

n	Q	E
010	255.56	0
020	347.925	-2.84×10^{-3}
030	393.5	-2.72×10^{-3}
100	326.0	-43.34×10^{-3}

TABLE VI
(See Fig. 18)

PRE-RUN

n	t(min.)	f_u	f_L	f_r	Q	E
010	0	564.45	562.07	563.26	238	0
020	7	1130.47	1127.38	1128.9	365	1.97×10^{-3}
030	4	1697.7	1693.7	1695.7	424	3.43×10^{-3}
100	10	1139.56	1136.2	1137.8	339	9.79×10^{-3}

FINITE-AMPLITUDE RUN

t(min.)	f(Hz)	V_2 (dB)	V_3 (dB)	V_2/V_1	V_3/V_1	FP
16	558.0	-44.2	-	0.0051	-	-4.69
19	558.3	-43.4	-	0.0056	-	-4.47
22	558.6	-42.8	-	0.006	-	-4.24
25	558.9	-42.9	-	0.0059	-	-4
28	559.2	-42.1	-	0.0065	-	-3.79
31	559.5	-41.9	-	0.0067	-	-3.57
34	559.8	-41.4	-	0.007	-	-3.35
37	560.1	-40.6	-	0.0078	-	-3.13
40	560.4	-40.2	-	0.0081	-	-2.9
43	560.7	-39.9	-	0.0084	-	-2.68
46	561.0	-39.3	-	0.009	-	-2.45
49	561.3	-38.9	-	0.0095	-	-2.23
52	561.6	-38.5	-	0.0099	-	-2.01
55	561.9	-38.1	-	0.01	-	-1.79
58	562.2	-37.6	-	0.011	-	-1.56
61	562.5	-37.3	-	0.0113	-	-1.34
64	562.8	-36.2	-	0.013	-	-1.12
67	563.1	-35.4	-	0.014	-	-0.89
70	563.4	-34.2	-	0.016	-	-0.67
73	563.7	-33.1	-	0.018	-	-0.45
76	564.0	-31.9	-55.9	0.021	0.0013	-0.22
79	564.3	-31	-54.1	0.023	0.0016	0
82	564.6	-29.8	-52.0	0.027	0.0021	0.2
85	564.9	-28.2	-49.8	0.032	0.0027	0.44
88	565.2	-27.1	-47.6	0.037	0.0034	0.67
91	565.5	-25.9	-45.1	0.042	0.0046	0.89
94	565.8	-25.1	-42.7	0.046	0.006	1.11
97	566.1	-24.8	-40.8	0.048	0.0076	1.34
100	566.4	-25.6	-39.3	0.044	0.009	1.56
103	566.7	-27.1	-39.0	0.037	0.0093	1.78
106	567.0	-29.2	-39.7	0.029	0.0086	2.00
109	567.3	-31.1	-41.4	0.023	0.007	2.23
112	567.6	-32.9	-44	0.019	0.0052	2.45
115	567.9	-34.2	-47.1	0.016	0.0036	2.67
118	568.2	-35.6	-49.4	0.014	0.0028	2.89
121	568.5	-37.1	-51.4	0.012	0.0022	3.12

TABLE VI (Cont.)

t(min.)	f(Hz)	V ₂ (dB)	V ₃ (dB)	V ₂ /V ₁	V ₃ /V ₁	FP
124	568.8	-38.5	-53.1	0.0099	0.0018	3.34
127	569.1	-39.2	-54.0	0.0091	0.0017	3.56
130	569.4	-39.5	-54.9	0.0088	0.0015	3.79
133	569.7	-39.1	-56.0	0.0092	0.0013	4.0
136	570.0	-37.9	-57.1	0.0098	0.0012	4.23
139	570.3	-36.4	-58.3	0.0126	0.001	4.45
142	570.6	-35.0	-59.0	0.0148	-	4.68
145	570.9	-35.9	-	0.0133	-	4.9
148	571.2	-36.8	-	0.012	-	5.12
151	571.5	-39.0	-	0.0093	-	5.34
154	571.8	-41.2	-	0.0072	-	5.57
157	572.1	-43.3	-	0.0057	-	5.79

POST-RUN

n	t(min.)	f _u	f _L	f _r	Q	E
010	156	566.48	564.18	565.33	245.8	0
020	159	1134.45	1131.25	1132.85	354	1.88 x 10 ⁻³
030	158	1703.75	1699.79	1701.77	429	3.34 x 10 ⁻³
100	160	1143.47	1139.97	1141.7	326	9.67 x 10 ⁻³

AVERAGE VALUES OF Q'S AND E'S

n	Q	E
010	242.0	0
020	359.5	1.93 x 10 ⁻³
030	426.5	3.39 x 10 ⁻³
100	332.5	9.73 x 10 ⁻³

TABLE VII
(See Fig. 19)

PRE-RUN

n	t(min.)	f_u	f_L	f_r	Q	E
010	0	565.89	563.58	564.735	244.47	0
020	6	1131.45	1128.46	1129.955	377.9	5.27×10^{-4}
030	3	1696.48	1692.69	1694.85	447.1	4.07×10^{-4}
100	8	1138.89	1135.78	1137.335	365.7	7.07×10^{-3}

FINITE-AMPLITUDE RUN

t(min.)	f(Hz)	V_2 (dB)	V_3 (dB)	V_2/V_1	V_3/V_1	FP
17	562.4	-32.9	-	0.0188	-	-2.05
20	562.7	-31.8	-	0.0214	-	-1.69
23	563.0	-30.3	-	0.0254	-	-1.4
26	563.3	-28.6	-48.6	0.031	0.003	-1.11
29	563.6	-26.7	-46.9	0.0385	0.00376	-0.81
32	563.9	-24.8	-44.0	0.0479	0.00526	-0.51
35	564.2	-22.8	-39.7	0.06	0.00863	-0.21
38	564.5	-21.3	-36.6	0.0797	0.0123	0.07
41	564.8	-21.0	-36.6	0.0742	0.0123	0.36
44	565.1	-21.6	-39.8	0.0693	0.00852	0.67
47	565.4	-23.5	-43.5	0.0557	0.00557	0.98
50	565.7	-25.0	-45.4	0.0468	0.00463	1.25
53	566.0	-26.8	-47.8	0.038	0.00339	1.56
56	566.3	-28.6	-49.0	0.031	0.00295	1.86
59	566.6	-30.1	-50.4	0.026	0.0025	2.15
62	566.9	-31.5	-51.8	0.022	0.0021	2.47
65	567.2	-32.8	-	0.019	-	2.76
68	567.5	-34.1	-	0.0164	-	3.04
71	567.8	-35.1	-	0.0146	-	3.33
74	568.1	-36.5	-	0.0124	-	3.62
77	568.4	-37.9	-	0.0106	-	3.92
80	568.7	-39.9	-	0.0084	-	4.23
83	569.0	-43.6	-	0.0055	-	4.52
86	569.3	-45.1	-	0.0046	-	4.83
89	569.6	-45.4	-	0.0044	-	5.12
92	569.9	-45.1	-	0.0046	-	5.41
95	570.2	-42.7	-	0.0061	-	5.7
98	570.5	-39.7	-	0.0086	-	6.01
101	570.8	-37.5	-	0.0111	-	6.3
104	571.1	-36.7	-	0.0121	-	6.6
107	571.4	-35.8	-	0.0135	-	6.9
110	571.7	-35.4	-	0.0141	-	7.2
113	572.0	-35.2	-	0.0145	-	7.49
116	572.3	-35.5	-	0.0139	-	7.78
119	572.6	-35.5	-	0.0139	-	8.07
122	572.9	-35.2	-	0.0145	-	8.37
125	573.2	-34.9	-	0.0149	-	8.68
128	573.5	-34.5	-	0.0156	-	8.97

TABLE VII (Cont.)

POST-RUN

n	t(min.)	f_u	f_L	f_r	Q	E
010	129	564.67	562.58	563.625	269.67	0
020	132	1129.57	1126.5	1128.035	367.44	7×10^{-4}
030	130	1693.6	1689.77	1691.685	441.70	4.52×10^{-4}
100	133	1136.98	1133.87	1135.425	365.08	7.26×10^{-3}

AVERAGE VALUES OF Q'S AND E'S

n	Q	E
010	257	0
020	372.67	6.135×10^{-4}
030	444.4	4.295×10^{-4}
100	365.39	7.165×10^{-3}

TABLE VIII
(See Fig. 21)

PRE-RUN

n	t(min.)	f_u	f_L	f_r	Q	E
010	0	564.79	562.56	563.675	253	0
020	9	1131.79	1128.8	1130.3	378	2.53×10^{-3}
030	3	1694.37	1691.66	1693.5	456.5	1.45×10^{-3}
100	11	1137.35	1134.19	1135.8	359	7.38×10^{-3}

FINITE-AMPLITUDE RUN

t(min.)	f(Hz)	V_2 (dB)	V_3 (dB)	V_2/V_1	V_3/V_1	FP
18	561.0	-29.2	-	0.0095	-	-2.55
21	561.3	-38.9	-	0.0099	-	-2.29
24	561.6	-38.1	-	0.0103	-	-2.04
27	561.9	-37.9	-	0.011	-	-1.78
30	562.2	-37.6	-	0.0114	-	-1.53
33	562.5	-37.4	-	0.0117	-	-1.27
36	562.8	-36.4	-	0.013	-	-1.02
39	563.1	-35.3	-	0.0149	-	-0.76
42	563.4	-34.3	-	0.0167	-	-0.51
45	563.7	-33.2	-51.6	0.019	0.0023	-0.26
48	564.0	-32.1	-48.9	0.022	0.003	0
51	564.3	-30.7	-45.5	0.025	0.0046	0.26
54	564.6	-29.4	-42.3	0.029	0.0067	0.51
57	564.9	-28.0	-40.8	0.035	0.0079	0.77
60	565.2	-26.9	-40.6	0.039	0.0081	1.02
63	565.5	-26.0	-41.4	0.043	0.0074	1.28
66	565.8	-26.2	-43.6	0.042	0.0057	1.53
69	566.1	-28.2	-46.1	0.034	0.0043	1.88
72	566.4	-30.4	-48.4	0.026	0.0033	2.13
75	566.7	-32.7	-50.1	0.02	0.0027	2.38
78	567.0	-34.5	-50.5	0.016	0.0025	2.64
81	567.3	-35.0	-	0.0154	-	2.89
84	567.6	-34.5	-	0.0163	-	3.15
87	567.9	-32.4	-	0.021	-	3.4
90	568.2	-30.8	-	0.025	-	3.66
93	568.5	-31.0	-	0.024	-	3.92
96	568.8	-31.6	-	0.023	-	4.16
99	569.1	-33.3	-	0.019	-	4.4
102	569.4	-35	-	0.0154	-	4.66
105	569.7	-36.9	-	0.0124	-	4.92

TABLE VIII (Cont.)

POST-RUN

n	t(min.)	f_u	f_L	f_r	Q	E
010	106	565.45	563.29	564.4	261	0
020	110	1133.07	1130.06	1131.6	376	2.44×10^{-3}
030	108	1697.48	1693.66	1695.6	444	1.38×10^{-3}
100	112	1138.67	1135.58	1137.1	368	7.28×10^{-3}

AVERAGE VALUES OF Q'S AND E'S

n	Q	E
010	257	0
020	377	2.485×10^{-3}
030	450	1.42×10^{-3}
100	363	7.33×10^{-3}

TABLE IX
(See Fig. 22)

PRE-RUN

n	t(min.)	f_u	f_L	f_r	Q	E
010	0	567	564.78	565.9	255	0
020	5	1132.66	1129.56	1131.1	364.8	-6.7×10^{-4}
030	3	1700.37	1696.56	1698.5	445.8	4.35×10^{-4}
100	7	1139.90	1136.38	1138.1	323.3	5.47×10^{-3}

FINITE-AMPLITUDE RUN

t(min.)	f(Hz)	V_2 (dB)	V_3 (dB)	V_2/V_1	V_3/V_1	FP
11	563.9	-29.4	-51.7	0.029	0.0022	-1.88
14	564.2	-27.7	-51.0	0.036	0.0024	-1.63
17	564.5	-26.4	-50.4	0.042	0.0026	-1.38
20	564.8	-24.8	-49.3	0.05	0.003	-1.12
23	565.1	-23.1	-47.1	0.061	0.0039	-0.87
26	565.4	-22.4	-43.9	0.067	0.0056	-0.63
29	565.7	-21.7	-40.4	0.072	0.0087	-0.38
32	566.0	-21.9	-38.1	0.07	0.011	-0.13
35	566.3	-24	-38.2	0.055	0.011	0.13
38	566.6	-25.1	-40	0.049	0.0087	0.38
41	566.9	-26.8	-43.4	0.04	0.0059	0.62
44	567.2	-28.2	-46.6	0.034	0.004	0.89
47	567.5	-29.9	-48.4	0.028	0.0033	1.12
50	567.8	-30.7	-50.2	0.025	0.0027	1.38
53	568.1	-31.2	-51.1	0.024	0.0024	1.63
56	568.4	-31.8	-	0.0225	-	1.87
59	568.7	-32.2	-	0.0215	-	2.13
62	569.0	-32.8	-	0.02	-	2.37
65	569.3	-33.6	-	0.018	-	2.62
68	569.6	-34.5	-	0.016	-	2.87
71	569.9	-35.6	-	0.0145	-	3.13
74	570.2	-36.6	-	0.0129	-	3.38
77	570.5	-37.1	-	0.0122	-	3.61
80	570.8	-38.1	-	0.01	-	3.87

POST-RUN

n	t(min.)	f_u	f_L	f_r	Q	E
010	76	567.58	565.38	566.98	257.49	0
020	82	1133.8	1130.68	1132.24	362.9	-7×10^{-4}
030	79	1702.01	1698.28	1700.15	455.8	3.82×10^{-4}
100	84	1140.75	1137.55	1139.15	335.9	5.39×10^{-3}

TABLE IX (Cont.)

AVERAGE VALUES OF Q'S AND E'S

n	Q	E
010	256.25	0
020	363.85	-6.85×10^{-4}
030	450.8	4.085×10^{-4}
100	339.6	5.43×10^{-3}

TABLE X
(See Fig. 24)

PRE-RUN

n	t (min.)	f_u	f_L	f_r	Q	E
010	0	564.95	562.8	563.9	269.8	0
020	3	1129.48	1126.58	1127.93	388.97	11.53×10^{-5}
030	2	1695.87	1691.96	1693.9	433	13×10^{-4}
100	5	1134.78	1131.76	1133.27	375.3	4.85×10^{-3}

FINITE-AMPLITUDE RUN

t (min.)	f (Hz)	V_2 (dB)	V_3 (dB)	V_2/V_1	V_3/V_1	FP
8	562.0	-32.0	-	0.0228	-	-0.92
11	562.3	-31.6	-	0.0239	-	-0.79
14	562.6	-30.9	-	0.0259	-	-0.65
17	562.9	-29.1	-52.4	0.0318	0.0022	-0.52
20	563.2	-27.5	-50.7	0.0383	0.00265	-0.38
23	563.5	-25.5	-47.5	0.0483	0.00383	-0.25
26	563.8	-23.8	-44.0	0.0587	0.00574	-0.12
29	564.1	-22.9	-40.9	0.065	0.0082	0.02
32	564.4	-22.9	-39.3	0.065	0.00985	0.15
35	564.7	-24.0	-42.7	0.0573	0.0093	0.28
38	565.0	-25.5	-46.2	0.0483	0.00666	0.42
41	565.3	-27.2	-48.7	0.0396	0.00445	0.55
44	565.6	-28.6	-50.2	0.0337	0.00333	0.69
47	565.9	-30.0	-51.7	0.0287	0.0028	0.82
50	566.2	-31.8	-52.4	0.0233	0.00218	0.95
53	566.5	-32.5	-	0.0215	-	1.08
56	566.8	-33.7	-	0.0188	-	1.21
59	567.1	-34.6	-	0.0169	-	1.35
62	567.4	-35.8	-	0.0147	-	1.48
65	567.7	-36.6	-	0.0134	-	1.62
68	568.0	-36.8	-	0.0131	-	1.75
71	568.3	-37.4	-	0.0123	-	1.88
74	568.6	-37.8	-	0.0117	-	2.02
77	568.9	-38.2	-	0.0111	-	2.15
80	569.2	-38.7	-	0.105	-	2.29
83	569.5	-39.8	-	0.0093	-	2.42
86	569.8	-40.8	-	0.0083	-	2.55

POST-RUN

n	t (min.)	f_u	f_L	f_r	Q	E
010	87	565.48	563.35	564.42	264.9	0
020	89	1130.42	1127.43	1128.9	373.6	5.3×10^{-5}
030	88	1697.15	1693.38	1695.27	449.7	11.87×10^{-4}
100	91	1135.71	1132.63	1134.17	368.23	4.72×10^{-3}

TABLE (Cont.)

AVERAGE VALUES OF Q'S AND E'S

n	Q	E
010	267.35	0
020	383	8.415×10^{-5}
030	441	12.435×10^{-4}
100	372	4.785×10^{-3}

TABLE XI
(See Fig. 25)

PRE-RUN

n	t(min.)	f_u	f_L	f_r	Q	E
010	0	562.685	560.65	561.6675	276	0
020	5	1126.73	1123.86	1125.295	392	16.3×10^{-4}
030	3	1688.36	1684.95	1686.555	467.2	8.6×10^{-4}
100	7	1130.85	1127.96	1129.4	310	5.23×10^{-3}

FINITE-AMPLITUDE RUN

t(min.)	f(Hz)	V_2 (dB)	V_1 (dB)	V_2/V_1	V_3/V_1	FP
10	567.0	-44.4	-	0.00574	-	5.11
13	566.7	-43.1	-	0.00666	-	4.78
16	566.4	-42.0	-	0.00756	-	4.438
19	566.1	-41.3	-	0.0082	-	4.1
22	565.8	-37.8	-	0.0122	-	3.77
25	565.5	-33.7	-	0.0196	-	3.436
28	565.2	-31.8	-	0.0244	-	3.1
31	564.9	-31.2	-51.3	0.0265	0.00259	2.77
34	564.6	-31.2	-50.1	0.0265	0.0297	2.43
37	564.6	-29.9	-49.0	0.03	0.00338	2.1
40	564.3	-28.2	-46.5	0.037	0.0045	1.77
43	564.0	-26.3	-44	0.046	0.006	1.43
46	563.7	-25.5	-41.7	0.0505	0.0078	1.099
49	563.4	-26.2	-40.9	0.0466	0.00858	0.765
52	563.1	-28	-40.7	0.0379	0.0087	0.47
55	562.8	-29.9	-43	0.0305	0.00674	0.088
58	562.5	-31.2	-47.1	0.0262	0.0042	-0.24
61	562.2	-32.6	-51.5	0.022	0.0025	-0.58
64	561.9	-33.6	-	0.0198	-	-0.91

POST-RUN

n	t(min.)	f_u	f_L	f_r	Q	E
010	72	563.67	561.63	562.65	275.8	0
020	76	1128.68	1125.86	1127.27	399.7	16.79×10^{-4}
030	74	1691.28	1687.73	1689.5	475.9	8.64×10^{-4}
100	77	1132.84	1129.97	1131.4	394.2	5.31×10^{-3}

AVERAGE VALUES OF Q'S AND E'S

n	Q	E
010	275.9	0
020	395.85	16.55×10^{-4}
030	471.55	8.62×10^{-4}
100	392.1	5.27×10^{-3}

TABLE XII
(See Fig. 27)

PRE-RUN

n	t(min.)	f_u	f_L	f_r	Q	E
010	0	565.08	563.07	564.075	280.6	0
020	4	1133.03	1130.12	1131.575	388.85	31.16×10^{-4}
030	3	1697.52	1693.79	1695.655	454.6	21.07×10^{-4}
100	5	1128.91	1125.79	1127.35	361.3	-6.47×10^{-4}

FINITE-AMPLITUDE RUN

t(min.)	f(Hz)	V_2 (dB)	V_3 (dB)	V_2/V_1	V_3/V_1	FP
17	561.0	-41.4	-	0.00826	-	-3.075
20	561.3	-39.4	-	0.0104	-	-2.8
23	561.6	-38.8	-	0.0111	-	-2.52
26	561.9	-39.3	-	0.0105	-	-2.25
29	562.2	-39.3	-	0.0105	-	-1.97
32	562.5	-39.1	-	0.0107	-	-1.695
35	562.8	-38.6	-	0.0114	-	-1.42
38	563.1	-38.1	-	0.01208	-	-1.14
41	563.4	-36.9	-	0.0138	-	-0.87
44	563.7	-34.7	-	0.078	-	-0.59
47	564.0	-31.5	-49.8	0.0258	0.00314	-0.32
50	564.3	-28.5	-48	0.0364	0.00386	-0.04
53	564.6	-27	-47.7	0.0433	0.004	0.24
56	564.9	-25.9	-47.8	0.0492	0.00396	0.51
59	565.2	-25	-48.8	0.0546	0.00352	0.79
62	565.5	-24.1	-52	0.0606	0.00244	1.07
65	565.8	-23.2	-47.9	0.0672	0.0039	1.35
68	566.1	-23.1	-43.3	0.0679	0.00663	1.63
71	566.4	-23.9	-42.4	0.0619	0.0073	1.89
74	566.7	-25.5	-43.6	0.0515	0.0064	2.18
77	567.0	-27.5	-45.4	0.0409	0.00515	2.44
80	567.3	-29.6	-48.0	0.0321	0.00386	2.72
83	567.6	-31.2	-50.0	0.0267	0.00307	3.00
86	567.9	-32.4	-51.7	0.0232	0.00252	3.28
89	568.2	-33.3	-52.9	0.0209	0.00219	3.56

POST-RUN

n	t(min.)	f_u	f_L	f_r	Q	E
010	91	565.63	563.58	564.605	275.42	0
020	95	1134.13	1131.2	1132.655	386.57	30.06×10^{-4}
030	93	1699.08	1695.56	1697.32	482.2	20.43×10^{-4}
100	97	1129.83	1126.85	1128.34	378.63	-8.32×10^{-4}

TABLE XII (Cont.)

AVERAGE VALUES OF Q'S AND E'S

n	Q	E
010	278	0
020	387.7	30.61×10^{-4}
030	468.4	20.75×10^{-4}
100	369.96	-7.4×10^{-4}

TABLE XIII
(See Fig. 28)

PRE-RUN

n	t(min.)	f_u	f_L	f_r	Q	E
010	0	560.4	558.36	559.38	274.2	0
020	6	1123.75	1120.83	1122.29	384.35	30.11×10^{-4}
030	3	1683.43	1679.91	1681.67	477.7	20.31×10^{-4}
100	8	1119.72	1116.71	1118.22	371.5	-7.15×10^{-4}

FINITE-AMPLITUDE RUN

t(min.)	f(Hz)	V_2 (dB)	V_3 (dB)	V_2/V_1	V_3/V_1	FP
13	555.0	-37.1	-	0.0093	-	-4.53
16	555.3	-37.4	-	0.00899	-	-4.28
19	555.6	-36.9	-	0.0095	-	-4.03
22	555.9	-36.5	-52.5	0.00997	0.00158	-3.77
25	556.2	-36.1	-52.4	0.0104	0.00159	-3.53
28	556.5	-35.9	-51.8	0.0107	0.0017	-3.28
31	556.8	-35.4	-52.6	0.0113	0.00156	-3.03
34	557.1	-35.1	-52.2	0.0117	0.00163	-2.78
37	557.4	-35.1	-52.4	0.0117	0.00163	-2.53
40	557.7	-34.5	-52.8	0.0125	0.00152	-2.82
43	558.0	-33.8	-52.6	0.0136	0.00156	-2.03
46	558.3	-33.1	-52.0	0.0148	0.00167	-1.77
49	558.6	-32.4	-52.0	0.0160	0.00167	-1.52
52	558.9	-32	-51.5	0.0167	0.00177	-1.28
55	559.2	-31.2	-51.0	0.0183	0.00187	-1.03
58	559.5	-30.1	-49.8	0.0208	0.00215	-0.79
61	559.8	-28.4	-47.5	0.025	0.0028	-0.54
64	560.1	-25.9	-45.1	0.0338	0.0037	-0.296
67	560.4	-23.4	-42.7	0.0445	0.00488	-0.04
70	560.7	-22.1	-41.1	0.0523	0.00587	0.21
73	561.0	-20.6	-39.1	0.0622	0.0074	0.45
76	561.3	-19.8	-37.6	0.0682	0.00878	0.71
79	561.6	-18.6	-36	0.078	0.0105	0.95
82	561.9	-17.6	-35	0.0879	0.0118	1.2
85	562.2	-16.9	-34.6	0.0952	0.0124	1.46
88	562.5	-16.5	-34.8	0.0997	0.0121	1.72
91	562.8	-16.9	-35.8	0.0952	0.0108	1.97
94	563.1	-17.7	-37.4	0.0868	0.00899	2.22
97	563.4	-19.1	-39.4	0.0739	0.00714	2.45
100	563.7	-20.4	-41.1	0.0639	0.00587	2.7
103	564.0	-21.4	-42.6	0.0567	0.00494	2.96
106	564.3	-23.1	-45.1	0.0466	0.0037	3.2
109	564.6	-23.8	-46.5	0.043	0.00315	3.46

TABLE XIII (Cont.)

POST-RUN

n	t(min.)	f_u	f_L	f_r	Q	E
010	100	561.97	559.96	560.97	279.1	0
020	104	1126.94	1123.95	1125.45	376.4	30.21×10^{-4}
030	102	1688.24	1684.68	1686.46	473.7	20.56×10^{-4}
100	107	1122.96	1119.88	1121.42	364.1	-6.4×10^{-4}

AVERAGE VALUES OF Q'S AND E'S

n	Q	E
010	276.65	0
020	380.4	30.16×10^{-4}
030	475.7	20.44×10^{-4}
100	367.8	-6.775×10^{-4}

BIBLIOGRAPHY

1. Coppens, A.B., and Sanders, J.V., "Finite-Amplitude Standing Waves in Rigid Walled Tubes," J. Acoust. Soc. Am., v. 43, p. 516-529, March 1968.
2. Coppens, A.B., and Sanders, J.V., "Finite-Amplitude Waves within Real Cavities," J. Acoust. Soc. Am., v. 58, p. 1133-1140, December 1975.
3. Lane, C., Finite-Amplitude Waves in a Rigid Walled Cavity, Thesis, Naval Postgraduate School, Monterey, California, 1972.
4. Devall, R.R., Finite Amplitude Waves in Imperfect Cavities, Thesis, Naval Postgraduate School, Monterey, California, 1973.
5. Slocum IV, W.S., Finite-Amplitude Standing Waves in Real Cavities Containing Degenerate Modes, Thesis, Naval Postgraduate School, Monterey, California, 1975.
6. Kirchhoff, G., Ann. Phys. Leipzig, v. 134, p. 177-193, 1868.
7. Lamb, H., Dynamical Theory of Sound, 2d ed., Chap. VI, Edward Arnold and Co., London, England, 1925.
8. Fay, R.D., "Plane Sound Waves of Finite Amplitude," J. Acoust. Soc. Am., v. 3, p. 222-241, 1931.
9. Fay, R.D., "Successful Method of Attack on Progressive Finite Waves," J. Acoust. Soc. Am., v. 28, p. 910-914, September 1956.
10. Keller, J.B., "Finite Amplitude Sound Produced by a Piston in a Closed Tube," J. Acoust. Soc. Am., v. 26, p. 253-254, 1954.
11. Keck, W., and Beyer, R.T., "Frequency Spectrum of Finite Amplitude Ultrasonic Waves in Liquids," Phy. Fluids, v. 3, p. 346-352, 1960.
12. Weston, D.E., Proc. Phys. Soc., (London) B66, p. 695-709, 1953.
13. Beech, W.L., Finite-Amplitude Standing Waves in Rigid Walled Tubes, Thesis, Naval Postgraduate School, Monterey, California, 1967.

14. Ruff, P.G., Finite Amplitude Standing Waves in Rigid Walled Tubes, Thesis, Naval Postgraduate School, Monterey, California, 1967.
15. Winn, J.R., Fourier Analysis of Experimental Finite Amplitude Standing Waves, Thesis, Naval Postgraduate School, Monterey, California, 1971.
16. Aydın, M., Theoretical Study of Finite-Amplitude Standing Waves in Rectangular Cavities with Perturbed Boundaries, Thesis, Naval Postgraduate School, Monterey, California, 1978.

INITIAL DISTRIBUTION LIST

	No. Copies
1. Defense Documentation Center Cameron Station Alexandria, Virginia 22314	2
2. Library, Code 0142 Naval Postgraduate School Monterey, California 93940	2
3. Department Library, Code 61 Department of Physics and Chemistry Naval Postgraduate School Monterey, California 93940	2
4. Professor James V. Sanders, Code 61Sd Department of Physics and Chemistry Naval Postgraduate School Monterey, California 93940	2
5. Professor Alan B. Coppens, Code 61Cz Department of Physics and Chemistry Naval Postgraduate School Monterey, California 93940	1
6. Lt. Ender Kuntsal Akatlar, Zeytinoğlu Caddesi Safak Ap. 240/16 Etiler, Istanbul/TURKEY	2
7. Lt. Mehmet Aydın Zincirlikuyu Caddesi No = 99 Kasımpaşa, Istanbul/TURKEY	1
8. Türk Deniz Kuvvetleri Komutanlığı Ankara, TURKEY	1
9. Dr. D.T. Blackstock Applied Research Laboratory University of Texas Austin, Texas 78712	1
10. Dr. Logan Hargrove Code 421, Physics Program, ONR, Ballston Centre Tower #1, Quincy Street, Washington, D.C. 20613	1

	No. Copies
11. Deniz Harp Okulu Komutanlığı Kütüphanesi Heybeliada, Istanbul/TURKEY	1
12. Istanbul Teknik Üniversitesi Kütüphanesi Taşkışla, Istanbul/TURKEY	1
13. Middle East Technical University Library Ankara, TURKEY	1
14. Boğaziçi Üniversitesi Kütüphanesi Bebek, Istanbul/TURKEY	1

Thesis
K8935
c.1

Kunsal

179395

Experimental study
of finite-amplitude
standing waves in rec-
tangular cavities with
perturbed boundaries.

Thesis
K8935
c.1

Kunsal

179395

Experimental study
of finite-amplitude
standing waves in rec-
tangular cavities with
perturbed boundaries.

thesK8935
Experimental study of finite-amplitude s



3 2768 002 11567 7
DUDLEY KNOX LIBRARY

C.1